Accepted Manuscript

Journal of the Geological Society

Cenozoic tectonic evolution of south-eastern Thailand derived from low-temperature thermochronology

Simon Nachtergaele, Stijn Glorie, Christopher Morley, Punya Charusiri, Pitsanupong Kanjanapayont, Pieter Vermeesch, Andrew Carter, Gerben Van Ranst & Johan De Grave

DOI: https://doi.org/10.1144/jgs2018-167

Received 5 September 2018
Revised 15 July 2019
Accepted 8 August 2019

Supplementary material at https://doi.org/10.6084/m9.figshare.c.4633064

To cite this article, please follow the guidance at http://www.geolsoc.org.uk/onlinefirst#cit_journal

Cenozoic tectonic evolution of south-eastern Thailand derived from low-temperature thermochronology

Simon Nachtergaele[1]*, Stijn Glorie[2], Christopher Morley[3], Punya Charusiri[4], Pitsanupong Kanjanapayont[4], Pieter Vermeesch[5], Andrew Carter[5], Gerben Van Ranst[1] & Johan De Grave[1]

[1]*Laboratory for Mineralogy and Petrology, Department of Geology, Ghent University, Belgium*

[2]*Centre for Tectonics, Resources and Exploration (TRaX), Department of Earth Sciences, School of Physical Sciences, University of Adelaide, Australia*

[3]*Petroleum Geophysics Program, Department of Geological Sciences, Chiang Mai University, Thailand*

[4]*Basin Analysis and Structural Evolution Special Task force for Activating Research (BASE STAR), Department of Geology, Chulalongkorn University, Bangkok, Thailand*

[5]*Department of Earth & Planetary Sciences, University College London, United Kingdom*

**Correspondence (Simon.Nachtergaele@UGent.be)*

Abstract: Low-temperature thermochronologic techniques, specifically apatite (U-Th)/He and apatite fission track dating were used to reconstruct the thermal history of south-eastern Thailand. This area is intersected by vast and complex fault networks related to the Cenozoic Mae Ping and Three Pagodas Faults. These were identified from satellite imagery and confirmed by field observations. New apatite fission track and apatite (U-Th)/He data were collected from crystalline basement blocks within these fault networks. Ages obtained range from 48 Ma to 24 Ma, with most of the samples clustering between 36 and 24 Ma. Thermal history modelling indicates late Eocene – Oligocene exhumation of the exposed granitic and metamorphic basement rocks in south-eastern Thailand. Exhumation was regional and was contemporaneous with sinistral fault activity during the late Eocene – early Oligocene along the Mae Ping Fault and Three Pagodas Fault. Moreover, this exhumation occurred coevally with a syn-rift phase of intracontinental offshore rift basin and half-graben basin development in the eastern Gulf of Thailand. The phase of exhumation ended in the early Miocene, as a result of the changing plate tectonic forces along the complex plate boundaries of Sundaland.

Keywords: Thailand, thermal history, apatite fission track dating, apatite (U-Th)/He dating, Sundaland, basin development

Supplementary material is available at https://doi.org/10.6084/m9.figshare.c.4633064

ORCID: 0000-0002-5451-4627

South-eastern Thailand is one of the critical areas for understanding the Indosinian orogeny because it contains good exposures of all three major tectonic terranes (Sibumasu, Sukhothai-Chantaburi, Indochina) and their intervening suture zones (Inthanon Zone, Nan-Sa Kaew suture) (Fig. 1, 2). Post-collision extension of uncertain age has also affected the area. Late Cretaceous-Cenozoic tectonics is particularly well-expressed in this area along an extensive network of strike-slip faults. In western Thailand the Mae Ping and Three Pagodas Fault Zones (Fig. 2, 3) are two major NW-SE trending, poorly dated strike-slip fault zones that have undergone sinistral motion at least during the late Eocene, with motion ending in the early Oligocene (Lacassin et al., 1997). These fault zones have possibly been affected by Late Cretaceous-Palaeogene transpressional deformation, and later movements related to escape tectonics, which include early sinistral motion and later dextral motion (Morley et al., 2011; Morley, 2012). Encountering south-eastern Thailand these strike-slip fault zones become broader, and exhibit a variety of geometries, including splays, horsetails, and duplexes (e.g. Morley, 2002; Morley et al., 2011, 2007, 2004). The region also borders the Gulf of Thailand, which has undergone a diachronous phase of rifting (Eocene-Miocene), followed by diachronous Miocene-Recent post-rift subsidence. Upton (1999) identified regional uplift-induced denudation or basement exhumation trends regionally across Thailand using apatite fission track (AFT) data (Appendix 1). Upton (1999) showed that most exhumation was of Cenozoic age, being generally older in the east (Palaeogene) and younger in the west (Neogene) (Appendix 1). However, south-eastern Thailand was very undersampled in his study (Fig. 3), hence the exhumation history of this particular region is poorly constrained. The issues concerning south-eastern Thailand that require an understanding of the exhumation history include: 1) what is the timing of the strike-slip faults and how does it compare with activity further west and east? 2) What effect did Cenozoic rifting and post-rift subsidence in the Gulf of Thailand have on exhumation of the adjacent onshore areas? 3) What are

the processes that contributed to exhumation of the Indosinian suture zones to the surface? 4) What is the influence of the Indosinian orogeny inherited structures on the basin formation history, both on- and offshore, and how are they related? Understanding the exhumation history, contributes a piece of information to the regional structural geological picture, which is necessary in order to gain deeper insights into the complex evolution of driving forces and their tectonic intraplate consequences and deformation history in the Sunda Plate (Sundaland) during the Cenozoic (Fig.1). Furthermore, the Sunda plate is a prime example of how rift basins and spreading centers develop diachronously and, suddenly stop due to a changing intraplate stress field.

This study combines observations from field work (Fig. 4) with low-temperature thermochronology to reconstruct the thermal history of south-eastern Thailand with emphasis on documenting the cooling of the basement rocks adjacent to the aforementioned faults in an absolute time frame. Here, we date the cooling of mainly granitoid basement through the upper crustal isotherms as a result of denudation of the overlying rock column; the latter caused by erosion or tectonic exhumation. The cooling history of the basement, and in particular the targeted deformed granitoids and metamorphosed rocks, places new constraints on the activity of the Mae Ping and Three Pagodas Faults as a response to regional or local plate tectonic forces. These long-lived strike-slip faults functioned as the principal crustal strain accommodators during phases of compressional and extensional stresses in northwestern Sundaland.

Geological setting

South-eastern Thailand comprises many low relief areas (100 m elevation or less) punctuated by NW-SE to NNW-SSE trending linear hills and ridges, where Cenozoic strike-slip faults have influenced the trends, and more oval, high relief areas are related to more erosion-resistant granitic plutons (Fig. 3). The highest relief is associated with the Khao Soi Dao Triassic pluton north of Chantaburi, where the highest peak exceeds 1600 m, but in general relief is less than 1000 m, and ridges in Palaeozoic and Mesozoic sedimentary, low-grade metamorphic, and volcanic units are commonly

300-500 m high. The study area is on the margin of the Gulf of Thailand, which is currently undergoing post-rift subsidence. The overall topographic expression suggests a region of previous uplift, with strong strike-slip control, that has been considerably eroded. Slow, ongoing subsidence has resulted in gradual infilling and onlap of the topography by recently deposited sediments.

Assembly of the basement units of Thailand

Our study area (Fig. 3) comprises three north-south oriented tectonic domains, that now form the basement of Thailand: Indochina in the east, Sibumasu (including the Inthanon Zone) to the west and the Sukhothai Arc in the centre (e.g. Metcalfe, 2011) (Fig. 2a). These terranes underwent several phases of granite intrusion, as a result of their accretionary history into the Sundaland collage, e.g. during the Triassic-Early Jurassic Indosinian Orogeny (Metcalfe 1996). These granite belts are traditionally subdivided in north-south oriented Eastern, Central and Western Granite Provinces and separated by suture zones (Hutchison 1975, 1977, 2007; Mitchell 1977) (Fig. 2a). The Indochina terrane rifted away from Gondwana during the Devonian and collided on its current northeastern side with South China in the Early Triassic (Lepvrier *et al.* 2004). Since the late Carboniferous – early Permian, the Nan-Sa Kaeo back-arc basin lay on the western side of the Indochina terrane, separating the Cathaysian Sukhothai arc from Indochina (Metcalfe 2013). The Nan-Sa Kaeo back-arc basin closed in the Early-Middle Triassic during the collision of the Sukhothai Arc with Indochina (Sone & Metcalfe 2008; Metcalfe 2013) as the Paleo-Tethys Ocean continued to close. The back-arc basin preserved early Permian to early-middle Triassic pelagic chert deposits, representative of deep-water environment (Sone *et al.* 2012). In our study area, remnants of these sequences with ophiolitic mélange such as bedded cherts, limestones, serpentinites, gabbros and pillow lavas are preserved in the (Nan-) Sa Kaeo (or Sra Kaew) suture zone (Hutchison 1975; Metcalfe 2000; Sone & Metcalfe 2008) (Fig. 2b, 5). West of the Nan-Sa Kaeo suture zone lies the Sukhothai volcanic arc, which is in its turn separated from the adjoining tectonic unit, i.e. the Sibumasu block by the so-called Klaeng tectonic line (Sone *et al.* 2012) (Fig. 2a, 2b, 5). Sibumasu was separated from

Gondwana in the late Early Permian and collided with the Sukhothai arc in the late Triassic – early Jurassic (e.g. Metcalfe 2013; Morley 2018) during the main phase of the Indosinian Orogeny and final Paleo-Tethys Ocean closure. The Inthanon Zone is thrust over the eastern part of the Sibumasu and represents the accretionary complex of the Indosinian orogeny (Barber *et al.* 2011; Ridd 2015). This accretionary complex underwent east-west compression and westwards thrusting as nappes during Indosinian accretion of Sibumasu (Ridd 2015). In eastern Thailand the Sibumasu block is located to the west of the Three Pagodas Fault and Khlong Marui Fault zone (Fig. 2a).

Long-lasting subduction of Paleo-Tethyan oceanic lithosphere from the Middle Devonian until the early Late Triassic (Sone & Metcalfe 2008) beneath Indochina is characterized by island arc and back-arc basin and magmatic arc development, that resulted in a belt of north-south aligned I-type (mantle-derived) granites (Eastern Granite Province) exposed across the Sukhothai arc and Indochina alike (Cobbing 2011; Searle *et al.* 2012; Metcalfe 2013). These I-type granites of the Eastern Granite Province are exposed in our study area (Fig. 2; 5) and typically yield late Triassic zircon U-Pb ages (Qian et al., 2017, and references therein). The Klaeng Fault "cryptic suture zone" contains mylonitic gneisses and migmatites (Sone *et al.* 2012), which seem to show peak metamorphism ages of 234 ± 3 Ma and 232 ± 2 Ma (Geard 2008) and constrain the collision and final closure of the Paleo-Tetyhan Ocean (Gardiner *et al.* 2016; Qian *et al.* 2017).

A large volume of S-type granites (Central Granite Province) intruded the Inthanon Zone when Sibumasu collided to the Sukhothai arc in the middle-early Late Triassic (Metcalfe 2013). The Central Granite Province covers the largest part of present-day Thailand and is exposed from the northern border of Thailand with Myanmar to the southern part of Thailand at its border with Malaysia (Cobbing 2011) (Fig. 1, 2). The part of the Central Granite Province located in our study area in south-eastern Thailand is called the Main Range Granite province, where it comprises the plutons of Rayong, Chonburi and Ban Na Cham (Cobbing, 2011). These granitoids are one of the main lithologies targeted for sampling in this study.

The Cretaceous S- and I-type granites of the Western Granite Province are located in the Sibumasu block (or Mogok-Mandalay-Mergui belt; Gardiner et al., 2015) to the west of our study area in Peninsular Thailand and Myanmar (Cobbing 1992; Gardiner *et al.* 2015).

In general, the granites that intruded into the Indochina terrane have more juvenile geochemical/isotopic characteristics, as indicated by positive zircon εNd values, while the Sibumasu block and the Inthanon Zone contain negative zircon εNd values, implying that the source for the latter granitoids was more evolved, and possibly pertains to recycled crust (Qian *et al.* 2017; Dew *et al.* 2018b, a). The Sukhothai Arc has intermediate zircon εNd values, indicative of a more hybrid crustal source (Dew *et al.* 2018b).

Late Mesozoic - Cenozoic tectonic evolution

During the Late Cretaceous – Eocene, an Andean-type margin developed in western Sundaland. Related events include the formation of supra subduction zone oceanic crust around 95 ± 2 Ma in the vicinity of the Andaman Islands (Pedersen *et al.* 2010; Pal 2011). Emplacement of large-scale I-type granite intrusions of Late Cretaceous-Palaeogene age in the Wuntho-Popa magmatic arc occurred, together with aforementioned S-type granites in the Mogok-Mandalay-Mergui belt (i.e. in Sibumasu basement) (Gardiner *et al.* 2015). While high-grade metamorphic complexes have yielded latest Cretaceous ages in the Doi Inthanon and Doi Suthep region (67-83 Ma), and the Lansang gneiss (70 Ma, Gardiner et al., 2016b) (Fig. 2), peak metamorphism alongside the Three Pagodas Fault is Palaeogene in age and occurred around 57-51 Ma in the Thabsila metamorphic complex (Fig. 2b; Nantasin et al., 2012). This metamorphism was accompanied by widespread I- and S-type granite emplacement in the Western Granite Province from the Late Cretaceous until the Eocene (e.g. Charusiri et al., 1993; Cobbing, 2011). This late metamorphism and even associated anataxis is clearly expressed in the Khao Chao region of our study area (Kawakami *et al.* 2014).

$^{40}Ar/^{39}Ar$ analyses constrained the termination of ductile sinistral deformation on the Three Pagodas fault in the latest Eocene (36 - 33 Ma) and the termination of ductile sinistral deformation along the

Mae Ping Fault zone in the earliest Oligocene (33 - 30 Ma) in western Thailand (Lacassin *et al.* 1997; Nantasin *et al.* 2012). This is followed by minor reactivation by dextral motion in the late Oligocene (Smith *et al.* 2007) or even an uplift-related event during the Oligocene – Miocene transition (~23Ma) (Lacassin *et al.* 1997), resulting in the current geometry of the Chainat Duplex (Smith *et al.* 2007) (Fig. 2b, 3). The south-eastern continuation of these two NW-SE to N-S oriented faults coincides with our study area (Morley *et al.* 2011) (Fig. 2b, 3). The Mae Ping Fault is thought to continue further eastwards and branches into numerous splays in Cambodia close to the Ton Le Sap Basin (Ridd & Morley 2011; Morley 2012) and further to the southeast into the Cuu Long basin, offshore Vietnam (Schmidt *et al.* 2019)(Fig. 2b). The Three Pagodas Fault zone south of Kanchanaburi splays into several trends including the N-S Ranong Fault and the more E-W trend that runs through Bangkok before curving to the NW-SE trend of the Klaeng Fault zone (Morley 2002; Ridd 2009) Fig. (2a, 2b, 3). The Ranong Fault shows episoidic activity, with an early phase before the Late Cretaceous (~81 Ma ago), based on $^{40}Ar/^{39}Ar$ and zircon U-Pb dating (Watkinson *et al.* 2011; Kanjanapayont *et al.* 2012), and together with the Khlong Marui Fault, underwent ductile dextral strike-slip shear from 47 Ma to 43 Ma, followed by a phase of brittle sinistral reactivation from 37 to 30 Ma (Watkinson *et al.* 2011). Apatite fission track data from Peninsular Thailand indicate final cooling through the isotherms around ~23 Ma for the current basement blocks, with exposed granites and gneisses along the Ranong Fault zone (Upton 1999; Blomme 2013; Nachtergaele *et al.* 2017). Further south, in Malaysia, crustal thickening in the Paleogene was followed by rapid cooling in the Eocene - late Oligocene, based on apatite fission track and apatite and zircon (U-Th)/He cooling ages (Krähenbuhl 1991; Cottam *et al.* 2013; Md Ali *et al.* 2016; François *et al.* 2017).

Geochronological information in south-eastern Thailand is rather limited to the aforementioned high-grade metamorphic rocks in the Klaeng fault zone (Geard, 2008; Kanjanapayont et al., 2013; Kawakami et al., 2014). Structural geological data from our study area suggests Eocene sinistral ductile deformation in the high-grade metamorphics in the Klaeng fault zone area (Geard 2008; Kanjanapayont *et al.* 2013). The Klaeng Fault gneisses are crosscut by leucogranites, with a Late

Cretaceous crystallization age (78.1 ± 0.7 Ma) (Cobbing 2011; Kanjanapayont *et al.* 2013). Sinistral ductile shearing post-dates leucogranites formed at 67 ± 1 and 72.1 ± 0.6 Ma (Kanjanapayont *et al.* 2013). The complex tectonic history of these mylonitic gneisses is further constrained by a U-Pb monazite age of 42.54 ± 0.88 Ma, and U-Pb titanite ages of 35.5 ± 3.1 Ma and 37.8 ± 4.8 Ma (Geard, 2008; Crow, 2011). All geochronological and structural geological evidence suggest that the Klaeng tectonic line (bounding the Sibumasu block in the west and the Sukhothai Arc in the east) experienced a complex and protracted history of reactivation and metamorphism during the Late Cretaceous and Cenozoic (Ridd 2012; Sone *et al.* 2012).

Post-Indosinian structures of south-eastern Thailand

While evidence for strike-slip control is clear from satellite images and geological maps (e.g. Ridd and Morley, 2011; Morley, 2012, Fig. 3), there is little published documentation of the structures from outcrop (Morley, 2012). However, one of the authors (CM) has found that strike-slip faults are commonly present in small, temporary exposures created while digging into hills for buildings or small aggregate quarries, all the way across the region from Chantaburi to north of Rayong (Fig. 4). Generally these are narrow, sub-vertical fault zones, marked by zones of cataclasis and gouge zones a few centimetres wide, and broader zones a few metres wide where bedding and/or foliations are sub-vertical and aligned parallel or sub-parallel to the fault zone (Fig. 4B). In Klaeng town a highly weathered NNW-SSE trending sinistral strike-slip mylonite zone was (temporarily) exposed in a building site, supporting the existence of the Klaeng Fault, which is primarily a feature interpreted from remote sensing images. The best exposed, more permanent strike-slip fault-related exposures are along the coast, in the Cretaceous Khao Thalai redbeds along the Khao Thalai Ridge (Thai Mai Fault) (Ridd and Morley, 2011; Morley, 2012). A quarry in the Khao Chao area shows a strand of the Klaeng Fault zone (Fig. 4C-F). This quarry exposes migmatites and leucogranites on the southern side of the fault, juxtaposed with amphibolites on the northern side (Fig. 4C,D). The fault zone is a narrow, brittle, transpressive, zone, with chlorite extensively distributed within the fault zone. The

biotite, garnet schists within the fault zone are strongly altered in part due to surface weathering, and in part due to fluid movement along the fault during deformation. In this particular case the brittle fault zone is later than the metamorphic fabric. The three terranes assembled during the Indosinian orogeny are all present in south-eastern Thailand, and are separated by two NNW-SSE trending suture zones (Inthanon Zone, and the Sa Kaeo suture, Sone et al., 2012). Therefore the study area for the low-temperature analyses in this work, holds a key position with respect to the broader tectonic architecture. The contacts within the zones appear to be highly disrupted by the later strike-slip faults.

East of Rayong there is a N-S trending, low-angled extensional mylonite zone several hundred metres thick, that has reworked the eastern margin of the large Triassic granite pluton complex that occupies much of the area between Rayong and Chonburi. In the hanging-wall of the top to the northeast granite mylonites, are flanked by schists and Permo-Triassic sedimentary units. Unconformably overlying these units is a less-deformed redbed sequence, of equivalent age to the Khorat Group (Jurassic-Cretaceous; Geard, 2008). The timing of extension is uncertain, and could range between the Latest Triassic and the Cenozoic. Major low-angle extensional events regionally are Late Triassic age (e.g. Late Triassic, basal Palaeozoic, Inthanon area, N. Thailand; Late Cretaceous, Stong Metamorphic Complex, N. Malaysia, ; Eocene, Khanom area, S. Thailand, Morley et al., 2011; and Late Oligocene-Early Miocene e.g. Doi Inthanon, N. Thailand see review in Morley et al., 2011).

Cenozoic basin evolution in the Gulf of Thailand

During the development of the oblique Andean-type margin from the Late Cretaceous to the Eocene, the crust in the Gulf of Thailand and adjacent areas became overthickened and hot (Morley, 2004; 2012; Gardiner et al., 2015; Palin et al., 2013). This overthickened crust in places experienced orogenic collapse in the late Eocene, leading to extension and basin development in the Gulf of Thailand. Conversely onshore parts of Thailand still experienced transpressional deformation,

related to major strike-slip fault activity in the late Eocene and Oligocene (Morley et al., 2011; Morley, 2012; Pubellier and Morley, 2014).

The offshore rift basins of the Gulf of Thailand are predominantly filled by continental deposits (Morley & Westaway 2006) attesting to the exhumation and erosion of adjoining continental basement blocks. Marine incursion periodically affected the Gulf of Thailand during the Miocene, and became more widespread and longer lived during the Pliocene-Recent (Morley & Westaway 2006). The basins of the Gulf of Thailand developed diachronously, whereby the basins located in the eastern Gulf of Thailand (i.e. northern Malay basin and Pattani basin; Fig. 2b) started to rift in the late Eocene and Oligocene and ceased around the Oligocene – Miocene transition (~23 Ma), followed by the deposition of kilometres of post-rift sediments on top of this syn-rift section (Morley & Racey 2011). This resulted in a minimal thickness of 7 km for the Pattani and North Malay basin (Morley & Racey 2011). However, the main phase of basin development in the south of the Gulf of Thailand (i.e. Chumphon, Nakhon, Songkhla, Khmer, North Malay and Pattani; Fig. 2b) lies in the Late Eocene, although in the deepest basins (i.e. North Malay and Pattani), it is problematic to observe the base of the sedimentary sections and biostratigraphic dating of the lowest stratigraphic levels lacks resolution (Heward *et al.* 2000; Morley & Racey 2011; Racey 2011; Morley 2015; Sautter *et al.* 2017).

In the western Gulf of Thailand, rifting initiated in the (late) Oligocene and continued in the early Miocene after rifting had already ceased in the eastern part of the Gulf (Morley & Racey 2011). Besides the diachronous onset of rifting, these basins contain more “anomalous” features which were discussed by Morley (2015), such as (1) the occurrence of low angle normal faults, (2) syn-rift episodes alternating with basin inversion, (3) rapid post-rift subsidence and (4) the occurrence of numerous, low-displacement post-rift faults. All of these anomalous features can be attributed to the characteristics of the underlying weak and hot crust in which they developed (Morley 2015). Lower crustal flow could explain the extreme thick post-rift sections in the Pattani and Malay Basins

in South East Asia, that accumulate up to 6 km and 12 km of syn- and post-rift sediments respectively (Morley & Westaway 2006).

Regional geological context of the Sunda plate

It has been suggested that a combination of stresses arising from collision zones (e.g. eastern Himalayas, Australia-Indonesia, Philippines), coupled with subduction slab-pull at the Java-Sunda-Sumatra trench, with associated subduction rollback and instability of the overthickened crust are the primarly controlling mechanisms that drive (extensional) basin development in Sundaland, and especially Thailand (Morley *et al.* 2000, 2001, 2004; Watkinson *et al.* 2008; Tingay *et al.* 2010; Searle & Morley 2011; Pubellier & Morley 2014) (Fig. 1, 2b). Subduction of oceanic lithosphere at the Java-Sunda-Sumatra trench was initiated around 45 Ma ago (Hall 2009). However, subduction initiation might be more diachronous than previously expected (Pubellier & Morley 2014). Following rifting in the Late Eocene- Oligocene, a drastic early Miocene change in stress orientation occurred (Pubellier & Morley 2014), and by the end of the early Miocene, almost all of the Sundaland basins stopped rifting, except for basins associated with the South Chinese Sea and the onshore Thailand basins (Pubellier & Morley 2014) as previously outlined. Extension during Oligocene to Early Miocene in the Andaman Sea developed in an east-west direction (Srisuriyon & Morley 2014). Subsequently, the direction of extension changed to a NNW-SSE direction in the Early to early Middle Miocene leading to a transtensional setting (Srisuriyon & Morley 2014).

The regional changes in stress orientation can be explained by a switch from subduction rollback and extensional collapse of the thickened lithosphere to transtension caused by the northwards movement of India towards Eurasia, tectonic coupling between India and Myanmar, and the Himalayan orogeny (Morley 2017). However, the effects of stress changes are different in the Andaman Sea, Gulf of Thailand and central and northern Thailand due to their different locations with respect to the sources of stress.

Samples and methods

The samples analysed in this study originate from onshore eastern Thailand gneiss and granite outcrops, located on the northeastern margins of the Gulf of Thailand (Table 1, Fig. 3). This area is intensively intersected by the fault networks related to the Mae Ping and Three Pagodas fault zones (Fig. 2b, 3, 5). Using a small sampling resolution, samples were collected from several plutons belonging to different Thai granite provinces (e.g. Cobbing, 1992) and therefore we could possibly evaluate potential differences in exhumation timing or exhumation rate along the different structural domains. Care was thus taken to sample several transects across the structural fabric and across known terrane boundaries. NT-01 and KM-01 are S-type granites from west of the Klaeng Fault line in the Main Range Central granite province of Thailand (Fig. 2a). KM-05 to KM-15 represent the Eastern granite Province (I-type) (Fig. 2a). Other samples were taken from several metamorphic basement inliers, such as NT-02 and KM-04 which are from the metamorphosed rocks at Khao Chao along the Klaeng fault zone, located in between the Main Range and Eastern granite provinces (Fig. 2a, 3). KM-04 originates from an area east of Rayong, and just north of Koh Samet, where paragneisses (Lem Khet Formation) from an Ordovican sedimentary protolith are exposed by low-angle normal faulting (Geard 2008; Morley *et al.* 2011). The migmatized granite sample KM-15 is the only sample located on the eastern side of the Sa Kaeo suture zone and is located on the main trace of the Mae Ping Fault (Fig. 2b, 3, 5).

Apatite fission track dating

Apatite fission track (AFT) dating is a low-temperature thermochronological method based on the spontaneous nuclear fission of ^{238}U, present as trace element in the crystal lattice of apatite. This fission process produces sub-microscopic linear radiation damage tracks (or fission tracks) in the apatite crystal lattice. These fission tracks are chemically etched with nitric acid in order to reveal the tracks for optical microscopic analysis at high magnification. At temperatures (T) lower than ca. 60°C, natural fission tracks in apatite are considered stable and are retained on geological time

scales, whereas at T > ~120°C the apatite crystal lattice regenerates and the fission tracks anneal rapidly (e.g. Ketcham et al., 1999; Wagner and Van den haute, 1992; Donelick et al., 2005). The ~60-120°C temperature window (corresponding to about 2-4 km crustal depth) represents the Apatite Partial Annealing Zone (APAZ) (Gleadow *et al.* 1986; Green *et al.* 1986). Here, tracks can accumulate but are progressively shortened, due to partial annealing at the track ends. The apatite fission track age, based on the measurement of the etched areal spontaneous fission track density is a cooling age, and hence dates the time since fission tracks became thermally stable.

All samples in this study were analysed with the external detector (ED) method using thermal neutron irradiation, following the standard procedure from the AFT laboratory at Ghent University (e.g. De Grave et al., 2011, 2009; De Grave and Van den haute, 2002; Glorie et al., 2010; Nachtergaele et al., 2018). Spontaneous fission tracks in apatite were etched in a 5.5 M nitric acid solution for 20 seconds at 21°C. After irradiation, induced tracks were revealed in the muscovite ED (Goodfellow, clear ruby) with 40% hydrofluoric acid (HF) for 40 min at 21°C. Irradiation was carried out in the Belgian Reactor 1 (BR1) (De Grave *et al.* 2010). AFT ages are calculated using the Overall Mean Weighted Zeta based on Durango and Fish Canyon Tuff apatite age standards and IRMM 540 glass dosimeter, and are reported as conventional mean zeta-ages (t_ζ) (Hurford & Green 1983; Hurford 1990) as well as central ages (t_c) (Galbraith 1990; Vermeesch 2009). The AFT length distribution is used for time-temperature history reconstruction by inverse thermal history modelling (Ketcham *et al.* 1999, 2007b; Gallagher 2012). Where possible, 100 horizontal confined tracks per sample were measured at 2000 × magnification with a Nikon Eclipse Ni-E microscope equipped with a DS-Ri2 camera (Fig. 6). For most of the samples, limited length data were available due to low spontaneous surface track densities and/or a low number of suitable grains. Hence, duplicate apatite mounts were made for ^{252}Cf-irradiation to enhance the number of confined tracks (Donelick & Miller 1991). Thermal history modelling was performed for NT-02 and KM-14B using the QTQt software (Gallagher 2012), with c-axis projection (Ketcham *et al.* 2007a) and using the Ketcham *et al.* (2007b) annealing equations and the Markov Chain Monte Carlo search method for

inverse modelling. Both samples (NT-02 and KM-14B) have enough track lengths (±100) so that the uncertainty for both thermal history models should be rather low (Barbarand *et al.* 2003). For samples with 40-100 track lengths, a thermal history is reconstructed and can be found in Appendix 5. During thermal history modelling, it was not possible to choose the appropriate geometry for each apatite crystal that was analysed during apatite (U-Th)/He analysis, because it is only possible to chose the sphere (2T), infinite slab, infinite cylinders and hexagonal fragments (1T) in QTQt (v5.6.0). Table 4 shows that erroneous F_T correction can lead to wrong corrected AHe ages and therefore we chose not to incorporate the apatite (U-Th)/He data in the thermal history model. The presented AFT data has been added as supplementary material 2 and the detailed procedure of thermal history modelling has been described in Appendix 4, which incorporates all necessary information in a standard format as proposed by various authors (Flowers *et al.* 2015; Gallagher 2016).

Apatite (U-Th)/He dating

Apatite (U-Th)/He (AHe) dating is also a low temperature dating technique and is based on the production (and diffusion and implantation) of α-particles (^{4}He nuclei) produced in the α-decay reaction series from ^{238}U, ^{235}U, ^{232}Th (and to a lesser extent ^{147}Sm) to their respective stable radiogenic daughters (^{206}Pb, ^{207}Pb, ^{208}Pb resp., and ^{143}Nd for ^{147}Sm) (Zeitler *et al.* 1987). The AHe dating technique has a presumed closure temperature of about ~70°C for cooling rates of 10°C/Ma (Ehlers & Farley 2003) and in that sense, is therefore complementary to the AFT method. An F_T correction factor for each isotope (^{238}U, ^{235}U and ^{232}Th) based on the geometry of the analysed apatite crystal is critical in order to correct the individual age for alpha-particle diffusion through the crystal lattice (Ketcham *et al.* 2011). The geometry can be cylindrical, hexagonal without pyramidal terminations (0T), one pyramidal termination (1T) or with 2 pyramidal terminations (2T) (see Ketcham et al. (2011)).

AHe analyses were performed in the London Geochronology Centre of University College London. ^{4}He measurements were done with the Pfeiffer Prisma 100 quadrupole mass spectrometry using a

^{3}He spike. Apatite grains encased in platinum crucibles were heated in vacuo to c. 850°C using an infrared laser system for 120 seconds, with a degassing time of 300 seconds and subsequently retrieved from the vacuum system. A secondary reheating and measuring step was applied for each aliquot, to detect possible incomplete degassing due to for example mineral inclusions. Following helium extraction the chamber is opened and aliquots are removed from the Cu planchet and placed into Teflon beakers. Subsequently the aliquots were dissolved in HNO_3, spiked with ^{230}Th and ^{235}U, and analysed for U and Th isotopes by Inductively Coupled Plasma Mass Spectrometry with an Agilent 7700x system. A blank vial of the HNO_3 digestive solution and vials of a U standard with known ^{238}U concentration were added to the ICP-MS run so that sample measurements can be calibrated. Reported He ages are corrected for α-ejection effects based on measured grain dimensions using the procedure of Ketcham et al. (2011). Each sample typically comprises four aliquots. Data reduction, error propagation and central age calculation were performed with HelioCalc (https://www.ucl.ac.uk/~ucfbpve/heliocalc/). More detailed information on the analytical procedures can be found in text appendix S1 of Wildman *et al.* (2017).

Results

Apatite fission track data

All our obtained apatite fission track (AFT) ages are Cenozoic and range from 48 to 23 Ma (Table 2), with the majority of central ages concentrated near the Eocene - Oligocene transition around ~33 Ma. Spontaneous track densities are low for almost all of the samples, due to a combination of the relatively young AFT ages and low U concentrations of the apatite grains (Table 2). Consequently, only around 20 confined tracks were found in most of the samples, producing only limited information on the track length distributions. For some samples, ^{252}Cf bombardment increased the number of measurable, horizontal fission tracks and these samples are indicated with an asterisk in Table 2. However, for sample NT-02 a total of 99 confined track lengths were measured, yielding a unimodal distribution with mean track length of 13.4 µm (Fig. 6). For KM-14B, the mean track length,

based on 134 lengths, is 13.3 µm but is slightly more negatively skewed than NT-02. The other samples show a small number of track lengths, but roughly confirm the observations from both previous samples, with mean track lengths that range from 12.7 to 14.6 µm and standard deviations ranging from 0.9 µm to 1.9 µm. Generally, all length-histograms have unimodal distributions with relatively long mean track lengths around 13-14 µm, in a few cases subtle negatively skewed and can be considered as typical for rapidly cooled basement samples (Fig. 6) (Gleadow *et al.* 1986). All samples pass the $P(\chi^2)$ homogeneity test, except for KM-01, KM-04 and KM-11A (Table 2). Radial plots with D_{par} measurements can be consulted in the Appendix 3 of this paper. The kinetic parameter D_{par} ranges from 1.12 to 1.83 µm for our samples, which is indicative of chlorine-poor apatite (Donelick 1993) that characteristically exhibit more rapid annealing of latent fission tracks (Green *et al.* 1986).

Apatite (U-Th)/He data

Four samples were prepared for apatite (U-Th)/He (AHe) dating. They all generally contain U-poor apatite grains (Table 3). F_T correction factors for ^{238}U, ^{235}U and ^{232}Th and F_T corrected ages were calculated with the HelioCalc software (Vermeesch; http://www.ucl.ac.uk/~ucfbpve/heliocalc/) based on each separate geometry (e.g. hexagonal 0T, hexagonal 1T, hexagonal 2T or cylindrical) of each analysed apatite crystal. Subsequently, some grains that degassed incompletely during laser fusion were discarded for further calculations (Table 3). Although an absolute minimum of apatite grains were analysed for each sample, consistent and reproducible ages were obtained, and a mean weighted AHe age was calculated for each of the samples. These weighted mean ages scatter between 33-25 Ma (Table 3). AHe mean weighted ages are within 1 standard error of their corresponding AFT central ages and are generally somewhat younger than the AFT age. Weighted mean age calculation was not possible for KM-15 because of significant outliers or incomplete degassing (Table 3). Only a single aliquot age of about 33.0 ± 1.0 Ma could thus be retained for this sample. Aliquot NT-02 (2) was not measured due to a technical problem during analysis. Over-

dispersed AHe ages (such as for KM-15) can be the result of several processes, such as the presence of U-rich inclusions (Stockli *et al.* 2000). Many fundamental questions concerning this over-dispersion still remain to be solved (Green & Duddy 2018; Van Ranst *et al.* 2019).

Thermal history modelling

The thermal history model for sample NT-02, based on its AFT age and length data (n=99), is well-constrained and indicates a two-staged thermal history. A rapid cooling phase is predicted to last until about 33 Ma, when slow cooling eventually brings the samples to ambient present-day surface temperatures. The mean weighted AHe age of 27.6 ± 1.5Ma for NT-02 is in excellent agreement with the thermal history model of NT-02, if we assume an AHe closure temperature of ~60-75°C. Moderate cooling, thus slower than for NT-02 is observed for KM-14B between 40 and 20 Ma (Fig. 7). Considering the relatively long mean track lengths of >13 µm in all samples (Fig. 7), except KM-01, and the occurrence of the 40 - 30 Ma cooling path in both reconstructed thermal history models, a late Eocene – earliest Oligocene rapid cooling event is clearly expressed in the data. The rapid cooling between 30-23 Ma could not be illustrated with thermal history models because of the low number of confined track length measurement. But, thermal history models of these samples are constructed and can be can be consulted in Appendix 5.

Discussion

Cenozoic exhumation-denudation history of Thailand

Low temperature thermochronometry techniques such as apatite fission track (AFT) and apatite (U-Th)/He (AHe) dating were applied on basement rocks originating from the Central and Eastern Granite Provinces. All AFT and AHe central ages are Eocene – Oligocene and range from 48 - 24 Ma, with most of the AFT and AHe ages concentrated around 36 - 24 Ma (late Eocene - Oligocene). Our data is in agreement with scarce existing low-temperature thermochronological data obtained on basement or sedimentary rocks in Thailand, which can be consulted in Appendix 1 (Putthapiban 1984; Racey *et al.* 1997; Upton 1999; Morley *et al.* 2007). For example an AFT age of 31 ± 3 Ma was

obtained on granitic basement (THI9430) in the northwest of our study area (Upton 1999) (Fig. 3). Our results are also comparable with unpublished AFT data of S. Meffre (reported in Morley et al., 2011) that indicate basement cooling from 38 - 22 Ma obtained from three granite samples in the Rayong fault zone area.Localized metamorphism in the Klaeng Fault strike-slip zone is constrained by monazite U-Pb ages of 42.54 ± 0.88 Ma and 35.5 ± 3.1 to 37.8 ± 4.8 Ma for titanite U-Pb (Geard 2008) and suggests a much later (Eocene) metamorphic overprint than previously suggested (Kawakami et al., 2014). Based on NW-SE shearing indicators and additional zircon U-Pb dating on deformed basement rocks exposed in this same area, ductile sinistral shearing of the Klaeng fault zone has been shown to have occurred after 67 ± 1 Ma (Kanjanapayont *et al.* 2013). Also, based on the unpublished monazite and titanite U-Pb ages of Geard (2008), an Eocene age for the NW-SE directed sinistral shearing was assumed. Our low-temperature thermochronometric data suggest that during this Eocene shearing, coeval basement exhumation brought the investigated rocks to upper crustal levels. Some of the AFT (KM-07, KM-08, KM-09) and AHe samples (KM-07, KM-09) suggest a latest phase of rock cooling during the Oligocene (Table 2 and 3) (Appendix 5, Fig. 8). At this time paleostress indicators show that shear senses shift to dextral (Lacassin *et al.* 1997).

Sample NT-02 from within the Klaeng Fault zone, yields a thermal history model exhibiting cooling before 33 Ma (Fig. 7). The AFT central age for sample NT-02 of 33.7 ± 1.8 combined with a unimodal, moderate to high mean track length value of 13.4 µm and two single grain AHe (F_T-corrected) ages of 25.4 ± 0.5 Ma and 29.7 ± 0.3 Ma indicate rapid cooling and associated final late Eocene – early Oligocene exhumation to shallow crustal levels of the metamorphosed rocks exposed in the Klaeng Fault zone (Khao Chao area). This hence immediately follows peak metamorphic conditions (Geard 2008). The migmatized granite KM-15 which is located on the main fault trace of the Mae Ping Fault system in the area has an AFT age of 33.0 ± 2.5 Ma, with a mean track length of 13.2 µm (based on 71 length measurements), and one AHe aliquot with an age of 33.1 ± 1.1 Ma and provided one retained, albeit incompletely degassed aliquot of 26.6 ± 3.6 Ma. This indicates fast cooling along the Mae Ping Fault zone around the Eocene – Oligocene transition and is in accordance with $^{40}Ar/^{39}Ar$

cooling ages from micas associated with the last phase of sinistral movement on the Three Pagodas Fault (36 - 33 Ma) further afield and the Mae Ping Fault zone (33 - 30 Ma) in western Thailand (Lacassin *et al.* 1997; Nantasin *et al.* 2012). The opening of the Cuu Long basin in south Vietnam, i.e. southeast of our study area, is also considered a direct consequence of sinistral fault activity of the Mae Ping fault zone from 40-31 Ma (Schmidt *et al.* 2019). Here also, a marked change to a dextral shear sense around 31-25 Ma is registered. The low T thermochronological data presented in this paper therefore connect both study areas (western Thailand and South Vietnam) and are in agreement with both proposed tectonic models.

The thermal history models presented here visualize how cooling of the basement rocks to shallower depths transpired. On the one hand, exhumation could be tectonic, as it is the case for basement rocks located in the hanging wall of low-angle faults controlling the opening of sedimentary basins for example. For example KM-04 is located in the hanging wall of an east dipping low-angle normal fault, identified by Geard (2008). Hence, the AFT age could represent the age of tectonic exhumation. On the other hand, AFT ages can also constrain the timing of erosional removal of the exhumed basement blocks. These basement blocks consequently provide source material for the developing, adjacent basins. Indeed, coarse conglomerates and breccias overlain by fluvial sandstones and fluvial and fluvial-deltaic mudstones are the typical sequence at the base of an offshore rift basin of the Gulf of Thailand (Morley and Racey, 2011). These coarse-grained deposits are interpreted as local erosion products originating from removal of rock-burden of uplifted areas. The cause of rapid exhumation along the strike-slip fault zones is probably related to erosion during thickening- and uplift in positive flower structures. Alternatively, the gravitational collapse that trigged extension in the Gulf of Thailand could have promoted a change from transpression to transtension along the strike-slip faults as well. In support of this model, extensional faults parallel to the strike of strike-slip faults in gneiss terrains are known from both the Mae Ping Fault zone in the Lansang national park (Lacassin et al., 1997) and from the Khao Chao area (Fig. 4A).

KM-14B lies west of the main Mae Ping Fault zone network, and east of the Three Pagodas Fault Zone network. Denudation and its associated basement cooling occurred between 32 Ma and present times, and has a slightly slower rate than for the previous sample (Figure 7). Strike-slip deformation in the region is very diffuse (Figure 3), hence the effects are likely to be a more gradual regional exhumation over a broad area, rather than focussed exhumation along a specific narrow strike-slip fault zone (in contrast with sample NT-02).

The late Oligocene AFT ages of KM-07 (23.9 ± 2.2 Ma), KM-08 (25.7 ± 1.9 Ma) and KM-09 (25.3 ± 2.5 Ma) and AHe ages for KM-07 (weighted mean: 25.0 ± 4.2 Ma) and KM-09 (weighted mean: 26.8 ± 2.4 Ma) obtained on the exposed plutons north of Chantaburi town, could indicate continued cooling in the late Oligocene through movement along the Tha Mai Fault (Fig. 5). The Tha Mai fault zone lies in the region of overlap between the branches of the Three Pagodas and the Mae Ping Fault zones (Ridd & Morley 2011) (Fig.5). Here, it might be the case that a phase of dextral movement along the Mae Ping and Three Pagodas fault zones exerts its influence on basement cooling. This has also been observed in the Chainat Duplex (Fig.2), where comparable late Oligocene – Miocene estimates of the timing of dextral motion along the Mae Ping fault took place (Smith *et al.* 2007). Further southeast in south Vietnam, estimations of dextral lateral motion from 31-25 Ma along the Mae Ping Fault responsible for a phase of compression in the Cuu Long basin (Schmidt *et al.* 2019).

The oldest AFT central ages found in the gathered low-temperature thermochronological dataset ofsamples KM-04 (45.5 ± 5.7 Ma) and KM-05 (48.3 ± 3.7 Ma) hint that there might be a South to North younging trend while both of them lie closest to the coast. This coincidence might suggest that the coastal region was exhumed first, and was also first to cease exhuming, followed by inland sites, which would fit with a rifting/thermal subsidence model, with the region of rifting located to the south. Admittedly, although our results hint at this possibility, more data should be collected to verify this model further. Another hypothesis to explain the “old” AFT ages in the southern coastal region is by speculating that the fault network of the Mae Ping and Three Pagodas Fault zones had

little influence during the Oligocene on the uplift history of KM-04 and KM-05. Perhaps, these granitic plutons were exhumed earlier during a late Cretaceous – Paleocene event which is now largely overprinted through later exhumation-denudation pulses in the Eocene – Oligocene. Low temperature thermochronologic data confirms that this event caused basement cooling in Cambodia in the Kampot Fold Belt (Fyhn *et al.* 2016). More geochronological evidence indicates metamorphism in this area during the Late Cretaceous – Palaeocene – Eocene. This is for example the zircon U-Pb ages from Kanjanapayont et al. (2013) as young as 67 ± 1 Ma and monazite U-Pb ages 43 ± 1 Ma from Geard (2008) from the Khao Chao gneisses and secondly, zircon U-Pb ages of 49.6 ± 0.9 to 47.2 ± 1.4 Ma from the Khao Chamao (15km east of the Khao Chao gneisses, i.e. KM-09 and KM-10) (Geard, 2008).

Further south of our study area in the eastern Gulf of Thailand, rifting ceased around 23 Ma in the Pattani, Khmer and Northern Malay basin (Morley 2015) (Fig. 2b). In the western Gulf of Thailand, an episode of basin inversion occurred in the Chumphon basin around 23 Ma and can be connected to cooling of granites and gneisses along the Ranong fault (Upton 1999). Recent reports of the Department of Mineral Fuels, Ministry of Energy (2018, Thailand) based on unpublished data indicate a phase of inversion at ~23 Ma (and in some cases even erosion) in all large basins of the Gulf of Thailand (Pattani, Northern Malay, Khmer, Songkhla, Chumphon, Kra, Western basin) (Department of Mineral Fuels, Ministry of Energy (2018, April 24). *Information memorandum, Thailand petroleum bidding round 2018 for offshore block G1/61&G2/61, Attachment 4.* Retrieved from http://bidding2018.dmf.go.th/G2/images/doc/IM_EN_Final.pdf). The cessation of rifting and subsequent onset of thermal subsidence in the eastern Gulf of Thailand ranges between about 23 Ma, and 10 Ma in the NW, consequently, such a diachronous event is unlikely to be represented by simple cooling age patterns onshore. However, overall the Late Eocene to late Oligocene low T thermochronologic ages overlap with the timing of opening of the basins offshore and phase of uplift at ~23Ma in the eastern Gulf of Thailand (Figure 8). After 23 Ma, when rifting ceased in the eastern Gulf of Thailand, few onshore exhumation occurred in onshore south-eastern Thailand.

In a broader context, the northern Mergui and northern Sumatra basins (Fig. 2b) ceased rifting around the late Oligocene – Early Miocene transition (~23Ma) (Morley 2017). The drastic stress change in Sundaland as a whole in the early Miocene is explained by cessation of sea floor spreading in the South China Sea and the end of subduction roll-back in the Java-Sunda-Sumatra trench (Pubellier & Morley 2014). In the early Miocene, there was a switch from subduction rollback and extensional collapse of the thickened lithosphere of Thailand, to transtension, caused by the northwards migration of India towards Eurasia and tectonic coupling between India and Myanmar (Morley 2017). Dextral motion along the Sagaing Fault (Myanmar) since the late Oligocene (28-27Ma) (Morley & Arboit 2019) is a direct consequence of the tectonic coupling between India and Myanmar. Our new late Eocene to late Oligocene low-temperature thermochronological data fit in this overall regional geodynamical picture, characterized by the opening of several on- and offshore basins and hence the contemporaneous cooling of the adjoining basement rocks, which is illustrated in Figure 7 and 8.

Importance of inherited structures

The north-south alignment of the sedimentary basins and strike-direction of the associated faults is controlled by zones of crustal weakness inherited from the Indosinian Orogeny (Morley *et al.* 2004, 2011). The recent hypothesis on continental rifting initiation indicates the requirement of pre-existing linear weaknesses and rotational extension (Molnar *et al.* 2018). The first requirement is fulfilled, since the majority of the intracontinental rift basins of the Gulf of Thailand are actually situated in pre-deformed lithospheric segments such as the Inthanon zone and Sukhothai Arc that have been deformed during the Indosinian orogeny (Fig. 2a, 2b). This zone experience a new phase of metamorphism in the Late Cretaceous – Eocene as a result of the Andean-type subduction west of Sibumasu (Searle *et al.* 2007; Gardiner *et al.* 2015), and therefore probably lost most of its lithospheric strength. The second requirement, i.e. the rotational extensional stress component initiated in the late Eocene due to slab pull forces at the Java-Sunda-Sumatra subduction zone since

45 Ma (Hall 2009), as India was obliquely colliding with Eurasia at that time. The influence of inherited orogenic structures on hot continental lithosphere undergoing extensional forces was investigated in a 2D numerical modelling approach by Balàzs et al. (2017). These authors modelled the effect of a lithospheric weak zone - representing a subducted slab of oceanic lithosphere - in the lithospheric mantle and subsequently calculated strain patterns in the lithosphere. The 2D geometry of the intracontinental rift basins caused by these extensional forces that would develop could be predicted. Extensional forces affecting the weakened lithosphere resulted in the development of sedimentary basins with normal syn-rift and post-rift evolution, but also in the development of some sedimentary basins with extreme amounts of post-rift subsidence. This situation of extreme post-rift subsidence is well-described in the Pattani, Kra and Northern Malay basin in the eastern Gulf of Thailand (Tjia 1994; Ngah *et al.* 1996; Morley & Westaway 2006; Morley & Racey 2011). The strain-based 2D modelling of Balàzs et al. (2017) showed that the presence of pre-existing orogenic structures in hot lithosphere causes the development of (1) asymmetric half-graben development bound by low angle normal faults during syn-rift evolution, (2) high post-rift subsidence in some of the developed basins, (3) asymmetrical asthenospheric upwelling leading to delayed mafic alkaline magmatism during post-rift and (4) uplift during initial extension and syn- to post-rift transition (Balàzs *et al.* 2017). Especially this latter feature comes into play when interpreting our data. The presented low-temperature thermochronological data (especially of sample KM-04) indicate that tectonic exhumation along low-angle normal faults occurred during initial extension in the region (~late Eocene) (Table 2; 3). The episodes of basin inversion around the Oligocene – Miocene transition (~23 Ma) also indicates significant exhumation on- and offshore during syn- to post-rift phase progression. Hence, these similarities show that the 2D strain-based modelling approach of Balàzs et al. (2017) has great potential and seems to be applicable in Thailand (and maybe entire Southeast Asia) for improving our understanding on basin development and in particular the anomalous features that characterize the Gulf of Thailand (e.g. as reviewed in Morley, 2015).

Further underscoring the broader implications of our observations, recent 3D strain-based modelling investigating the opening and propagation of the South China Sea explains the V-shaped nature of the oceanic rift by the influence of far-field tectonic effects (Le Pourhiet *et al.* 2018). Moreover, their modelling predicted that the width of the rift basins increased towards the propagator (Le Pourhiet *et al.* 2018), which is certainly the case for the Gulf of Thailand (Fig. 8). Strike-slip faults which make an angle of 45° with the direction of extension typically bound these rift basins (Le Pourhiet *et al.* 2018). These observations from this theoretical 3D model are comparable to the geometries of the rift basins characteristic of the eastern Gulf of Thailand (i.e. west of the South China Sea), which opened in the late Eocene and continued rifting until the late Oligocene. Numerous faults such as the Mae Ping and Three Pagodas Fault trend NW-SE while the Ranong and Khlong Marui fault zone trend NE-SW, which is both 45° on the east-west extensional direction in which the failed rift basins developed. A drastic change in spreading direction with 15° due to far-field tectonic driving forces occurred in the South China Sea at magnetic anomaly 6a (i.e. at 20.5 Ma) (Sibuet *et al.* 2016), which is contemporaneous with the transition to post-rift of the basin of the eastern Gulf of Thailand (Fig. 8, right panel).

Conclusions

Based on our new low-temperature thermochronological data and thermal history modelling on basement rocks in south-eastern Thailand, we could draw the following conclusions:

- The basement rocks of south-eastern Thailand experienced exhumation predominantly during the Late Eocene and Oligocene. Most apatite fission track and (U-Th)/He ages concentrate around 36 - 24 Ma, which is in agreement with previous estimates of the timing of exhumation along the major Mae Ping and Three Pagodas Fault zones. These estimates are related to late Eocene sinistral displacement along the Mae Ping and Three Pagodas fault zones, as already observed in Western Thailand and Southern Vietnam. During the late Oligocene, some of the sampled rocks experienced final

cooling as a results of the minor dextral motion along the Mae Ping and Three Pagodas fault zones.The syn-rift phase (Late Eocene to the Oligocene-Miocene transition) of the failed rift basins of the eastern Gulf of Thailand occurred simultaneously with onshore basement cooling and thus exhumation through the upper crust of south-eastern Thailand.

- Exhumation decreased in south-eastern Thailand after the Oligocene –Miocene transition (~23 Ma), under the influence of a changing regional stress pattern caused by larger-scale plate tectonic events in Sundaland. Specifically in the eastern Gulf of Thailand the change of the regional stress patterns is related to the cessation of rifting, and onset of thermal subsidence at around 23 Ma. Promising similarities between model and ground-truthing indicate that results from thermochronological studies maybe should be incorporated in lithospheric strain modelling studies in order to further test the geological reality with the model's predicted time-slices.

Acknowledgements

We would like to thank Mr. Peerasit Surakiatchai who assisted during field work. We are very grateful to Ann-Eline Debeer for assistance in the lab during mineral separations. James Schwanethal is acknowledged for development and maintenance of the apatite (U-Th)/He facilities at UCL. We would like to thank Bart Van Houdt and Dr. Guido Vittiglio for help during neutron irradiation at the Belgian Nuclear Research Centre in Mol (SCK-CEN, BR1 facility). We would like to thank Wenjiao Xiao for editorial work. This manuscript benefited from many useful suggestions from two anonymous referees, for which we are very grateful.

Funding

SN received a PhD Fellowship of the Research Foundation – Flanders (FWO). Funding for JDG was from a research grant from the Research Foundation – Flanders (FWO) number 31528111. SG's

contribution was supported by an Australian Research Council Discovery grant (DP150101730) and forms TRAX record 418. PK was funded by Ratchadaphiseksomphot Endowment Fund, Chulalongkorn University.

References

Balàzs, A., Burov, E., Matenco, L., Vogt, K., Francois, T. & Cloetingh, S. 2017. Symmetry during the syn- and post-rift evolution of extensional back-arc basins: The role of inherited orogenic structures. *Earth and Planetary Science Letters*, **462**, 86–98, https://doi.org/10.1016/j.epsl.2017.01.015.

Barbarand, J., Carter, A., Wood, I. & Hurford, T. 2003. Compositional and structural control of fission-track annealing in apatite. *Chemical Geology*, **198**, 107–137, https://doi.org/10.1016/S0009-2541(02)00424-2.

Barber, A.J., Ridd, M.F. & Crow, M.J. 2011. The origin, movement and assembly of the pre-Tertiary tectonic units of Thailand. *In*: Ridd, M. F., Barber, A. J. & Crow, M. J. (eds) *The Geology of Thailand*. The Geological Society of London, 507–537.

Blomme, K. 2013. *Apatite Fission Track Thermochronology and Petrographic Characterization of South Thailand Granitoids: Evolution of the Andaman Basin with Respect to the Eastern Indian Passive Margin (MSc Thesis)*. Ghent University.

Charusiri, P., Clark, A.H., Farrar, E., Archibald, D. & Charusiri, B. 1993. Granite belts in Thailand: evidence from 40Ar/39Ar geochronological and geological syntheses. *Journal of Southeast Asian Earth Sciences*, **8**, 127–136.

Cobbing, E.J. 1992. *The Granites of the South-East Asian Tin Belt*. HMSO.

Cobbing, E.J. 2011. Granitic Rocks. *In*: Ridd, M. F., Barber, A. J. & Crow, M. J. (eds) *The Geology of Thailand*. The Geological Society of London, 441–457.

Cottam, M.A., Hall, R. & Ghani, A.A. 2013. Late cretaceous and cenozoic tectonics of the Malay Peninsula constrained by thermochronology. *Journal of Asian Earth Sciences*, **76**, 241–257, https://doi.org/10.1016/j.jseaes.2013.04.029.

Crow, M.J. 2011. Appendix. Radiometric ages of Thailand rocks. *In*: Ridd, M. F., Barber, A. J. & Crow, M. J. (eds) *The Geology of Thailand*. The Geological Society of London, 593–614.

De Grave, J. & Van den haute, P. 2002. Denudation and cooling of the Lake Teletskoye Region in the Altai Mountains (South Siberia) as revealed by apatite fission-track thermochronology. *Tectonophysics*, **349**, 145–159.

De Grave, J., Buslov, M.M., van den Haute, P., Dehandschutter, B. & McWilliams, M.O. 2009. Multi-method chronometry of the Teletskoye graben and its basement, Siberian Altai Mountains: new insights on its thermo-tectonic evolution. *Geological Society, London, Special Publications*, **324**, 237–259, https://doi.org/10.1144/SP324.17.

De Grave, J., Glorie, S., Vermaercke, P., Vittiglio, G. & Van Den Haute, P. 2010. A " new " irradiation facility for FT applications at the Belgian Nuclear Research Centre : the BR1 reactor. *In*: *Thermo 2010*.

De Grave, J., Glorie, S., et al. 2011. The thermo-tectonic history of the Song-Kul plateau, Kyrgyz Tien Shan: Constraints by apatite and titanite thermochronometry and zircon U/Pb dating. *Gondwana Research*, **20**, 745–763, https://doi.org/10.1016/j.gr.2011.03.011.

Dew, R.E.C., Nachtergaele, S., et al. 2018a. Data analysis of the U – Pb geochronology and Lu – Hf system in zircon and whole-rock Sr , Sm – Nd and Pb isotopic systems for the granitoids of Thailand. *Data in Brief*, **21**, 1794–1809, https://doi.org/https://doi.org/10.1016/j.lithos.2018.09.019.

Dew, R.E.C., Collins, A.S., et al. 2018b. Probing into Thailand's basement : New insights from U – Pb geochronology, Sr, Sm – Nd, Pb and Lu–Hf isotopic systems from granitoids. *Lithos*, **320–321**, 332–354, https://doi.org/10.1016/j.lithos.2018.09.019.

Donelick, R.A. 1993. Apatite etching characteristics versus chemical composition. **96**, 62–66, https://doi.org/US005485919A.

Donelick, R.A. & Miller, D.S. 1991. Enhanced TINT fission track densities in low spontaneous track density apatites using 252Cf-derived fission fragment tracks: a model and experimental observations. *Nuclear tracks Radiation Measurements*, **18**, 301–307.

Ehlers, T.A. & Farley, K.A. 2003. Apatite (U-Th)/He thermochronometry: methods and applications to problems in tectonic and surface processes. *Earth and Planetary Science Letters*, **206**, 1–14.

Flowers, R.M., Farley, K.A. & Ketcham, R.A. 2015. A reporting protocol for thermochronologic modeling illustrated with data from the Grand Canyon. *Earth and Planetary Science Letters*, **432**, 425–435.

François, T., Md Ali, M.A., Matenco, L., Willingshofer, E., Ng, T.F., Taib, N.I. & Shuib, M.K. 2017. Late Cretaceous extension and exhumation of the Stong and Taku magmatic and metamorphic complexes, NE Peninsular Malaysia. *Journal of Asian Earth Sciences*, **143**, 296–314, https://doi.org/10.1016/j.jseaes.2017.04.009.

Fyhn, M.B.W., Green, P.F., et al. 2016. Cenozoic deformation and exhumation of the Kampot Fold Belt and implications for south Indochina tectonics. *Journal of Geophysical Research*, **121**, 5278–5307, https://doi.org/10.1002/2015JB012625.Received.

Galbraith, R.F. 1990. The radial plot: Graphical assessment of spread in ages. *International Journal of Radiation Applications and Instrumentation. Part*, **17**, 207–214, https://doi.org/10.1016/1359-0189(90)90036-W.

Gallagher, K. 2012. Transdimensional inverse thermal history modeling for quantitative thermochronology. *Journal of Geophysical Research: Solid Earth*, **117**, 1–16, https://doi.org/10.1029/2011JB008825.

Gallagher, K. 2016. Comment on ' A reporting protocol for thermochronologic modeling illustrated with data from the Grand Canyon ' by Flowers , Farley and Ketcham. *Earth and Planetary Science Letters*, **441**, 211–212, https://doi.org/10.1016/j.epsl.2016.02.021.

Gardiner, N.J., Searle, M.P., Robb, L.J. & Morley, C.K. 2015. Neo-Tethyan magmatism and metallogeny in Myanmar - An Andean analogue? *Journal of Asian Earth Sciences*, **106**, 197–215, https://doi.org/10.1016/j.jseaes.2015.03.015.

Gardiner, N.J., Searle, M.P., Morley, C.K., Whitehouse, M.P., Spencer, C.J. & Robb, L.J. 2016. The closure of Palaeo-Tethys in Eastern Myanmar and Northern Thailand: New insights from zircon U–Pb and Hf isotope data. *Gondwana Research*, **39**, 401–422,

https://doi.org/10.1016/j.gr.2015.03.001.

Geard, A. 2008. *Geology of the Klaeng Region (Southeast Thailand): Lithology, Structure and Geochronology. Unpublished BSc Hons Thesis*. University of Tasmania.

Gleadow, A.J.W., Duddy, I.R., Green, P.F. & Lovering, J.F. 1986. Confined fission track lengths in apatite: a diagnostic tool for thermal history analysis. *Contributions to Mineralogy and Petrology*, **94**, 405–415, https://doi.org/10.1007/BF00376334.

Glorie, S., De Grave, J., Buslov, M.M., Elburg, M.A., Stockli, D.F., Gerdes, A. & Van Den Haute, P. 2010. Multi-method chronometric constraints on the evolution of the Northern Kyrgyz Tien Shan granitoids (Central Asian Orogenic Belt): From emplacement to exhumation. *Journal of Asian Earth Sciences*, **38**, 131–146, https://doi.org/10.1016/j.jseaes.2009.12.009.

Green, P. & Duddy, I. 2018. Apatite (U-Th-Sm)/He thermochronology on the wrong side of the tracks. *Chemical Geology*, **488**, 21–33, https://doi.org/10.1016/j.chemgeo.2018.04.028.

Green, P.F., Duddyi, I.R., Gleadow, A.J.W., Tingate, P.R. & Laslett, G.M. 1986. Thermal annealing of fission tracks in apatite 1. A Qualitative description. *Chemical Geology*, **59**, 237–253.

Hall, R. 2009. Hydrocarbon basins in SE Asia: understanding why they are there. *Petroleum Geoscience*, **15**, 131–146, https://doi.org/10.1144/1354-079309-830.

Heward, A.P., Chuenbunchom, S., Mäkel, G., Marsland, D. & Spring, L. 2000. Nang Nuan oil field, B6/27, Gulf of Thailand: karst reservoirs of meteoric or deep-burial origin. *Petroleum Geoscience*, **6**, 15–27.

Hurford, A.J. 1990. Standardization of fission track dating calibration: Recommendation by the Fission Track Working Group of the I. U. G. S. Subcommission on Geochronology. *Chemical Geology*, **80**, 171–178.

Hurford, A.J. & Green, P.F. 1983. The zeta age calibration of fission-track dating. *Chemical Geology*, **41**, 285–317, https://doi.org/10.1016/S0009-2541(83)80026-6.

Hutchison, C.S. 1975. Ophiolite in Southeast Asia. *Bulletin of the Geological Society of America*, **86**, 797–806, https://doi.org/10.1130/0016-7606(1975)86<797:OISA>2.0.CO;2.

Hutchison, C.S. 1977. Granite emplacement and tectonic subdivision of Peninsular Malaysia. *Geological Society,Malaysia*, **9**, 187–207.

Hutchison, C.S. 2007. *Geological Evolution of South-East Asia*. Geological Society of Malaysia, https://doi.org/10.1016/0264-8172(91)90051-2.

Kanjanapayont, P., Klötzli, U., Thöni, M., Grasemann, B. & Edwards, M.A. 2012. Rb–Sr, Sm–Nd, and U–Pb geochronology of the rocks within the Khlong Marui shear zone, southern Thailand. *Journal of Asian Earth Sciences*, **56**, 263–275, https://doi.org/10.1016/j.jseaes.2012.05.029.

Kanjanapayont, P., Kieduppatum, P., Klötzli, U., Klötzli, E. & Charusiri, P. 2013. Deformation history and U-Pb zircon geochronology of the high grade metamorphic rocks within the Klaeng fault zone, eastern Thailand. *Journal of Asian Earth Sciences*, **77**, 224–233, https://doi.org/10.1016/j.jseaes.2013.08.027.

Kawakami, T., Nakano, N., et al. 2014. U-Pb zircon and CHIME monazite dating of granitoids and high-grade metamorphic rocks from the Eastern and Peninsular Thailand - A new report of Early Paleozoic granite. *Lithos*, **200–201**, 64–79, https://doi.org/10.1016/j.lithos.2014.04.012.

Ketcham, R.A., Donelick, R.A. & Carlson, W.D. 1999. Cariability of apatite fission-track anneling kinetics: III. Extrapolation to geological time scales. *American Mineralogist*, **84**, 1235–1255.

Ketcham, R.A., Carter, A., Donelick, R.A., Barbarand, J. & Hurford, A.J. 2007a. Improved measurement of fission-track annealing in apatite using c-axis projection. *American Mineralogist*, **92**, 789–798, https://doi.org/10.2138/am.2007.2280.

Ketcham, R.A., Carter, A., Donelick, R.A., Barbarand, J. & Hurford, A.J. 2007b. Improved modeling of fission-track annealing in apatite. *American Mineralogist*, **92**, 799–810, https://doi.org/10.2138/am.2007.2281.

Ketcham, R.A., Gautheron, C. & Tassan-Got, L. 2011. Accounting for long alpha-particle stopping distances in (U-Th-Sm)/He geochronology: Refinement of the baseline case. *Geochimica et Cosmochimica Acta*, **75**, 7779–7791, https://doi.org/10.1016/j.gca.2011.10.011.

Krähenbuhl, R. 1991. Magmatism, tin mineralization and tectonics of the Main Range, Malaysian Peninsula: Consequences for the plate tectonic model of Southeast Asia based on Rb-Sr, K-Ar and fission track data. *Geo. Soc. Malaysia, Bulletin*, **29**, 1–100.

Lacassin, R., Maluski, H., et al. 1997. Tertiary diachronic extrusion and deformation of western Indochina: structural and 40Ar/39Ar evidence from NW Thailand. *Journal of Geophysical Research*, **102**.

Le Pourhiet, L., Chamot-Rooke, N., Delescluse, M., May, D.A., Watremez, L. & Pubellier, M. 2018. Continental break-up of the South China Sea stalled by far-field compression. *Nature Geoscience*, **11**, 1–5, https://doi.org/10.1038/s41561-018-0178-5.

Lepvrier, C., Maluski, H., Van Tich, V., Leyreloup, A., Truong Thi, P. & Van Vuong, N. 2004. The Early Triassic Indosinian orogeny in Vietnam (Truong Son Belt and Kontum Massif); implications for the geodynamic evolution of Indochina. *Tectonophysics*, **393**, 87–118, https://doi.org/10.1016/j.tecto.2004.07.030.

Md Ali, M.A., Willingshofer, E., et al. 2016. Kinematics of post-orogenic extension and exhumation of the Taku Schist, NE Peninsular Malaysia. *Journal of Asian Earth Sciences*, **127**, 63–75, https://doi.org/10.1016/j.jseaes.2016.06.020.

Metcalfe, I. 1996. Pre-Cretaceous evolution of SE Asian terranes. *Geological society, London, Special Publications*, **106**, 97–122.

Metcalfe, I. 2000. The Bentong – Raub Suture Zone. *Journal of Asian Earth Sciences*, **18**, 691–712, https://doi.org/10.1016/S1367-9120(00)00043-2.

Metcalfe, I. 2011. Tectonic framework and Phanerozoic evolution of Sundaland. *Gondwana Research*, **19**, 3–21, https://doi.org/10.1016/j.gr.2010.02.016.

Metcalfe, I. 2013. Gondwana dispersion and Asian accretion: Tectonic and palaeogeographic evolution of eastern Tethys. *Journal of Asian Earth Sciences*, **66**, 1–33, https://doi.org/10.1016/j.jseaes.2012.12.020.

Mitchell, A.H.. 1977. Tectonic settings for emplacement of southeast asia tin granites. *Geological Society of Malaysia*, **9**, 123–140.

Molnar, N.E., Cruden, A.R. & Betts, P.G. 2018. Unzipping continents and the birth of microcontinents. *Geology*, **46**, 451–454, https://doi.org/10.1130/G40021.1.

Morley, C.K. 2002. A tectonic model for the Tertiary evolution of strike-slip faults and rift basins in SE Asia. *Tectonophysics*, **347**, 189–215, https://doi.org/10.1016/S0040-1951(02)00061-6.

Morley, C.K. 2012. Late Cretaceous-Early Palaeogene tectonic development of SE Asia. *Earth-Science Reviews*, **115**, 37–75, https://doi.org/10.1016/j.earscirev.2012.08.002.

Morley, C.K. 2015. Five anomalous structural aspects of rift basins in Thailand and their impact on petroleum systems. *Geological Society, London, Special Publications*, **421**, 143–168, https://doi.org/10.1144/SP421.2.

Morley, C.K. 2017. Cenozoic rifting, passive margin development and strike-slip faulting in the Andaman Sea: a discussion of established v. new tectonic models. *In*: *Geological Society, London, Memoirs*. 27–50., https://doi.org/10.1144/M47.4.

Morley, C.K. 2018. Understanding Sibumasu in the context of ribbon continents. *Gondwana Research*, **64**, 184–215, https://doi.org/10.1016/j.gr.2018.07.006.

Morley, C.K. & Arboit, F. 2019. Dating the onset of motion on the Sagaing fault: Evidence from detrital zircon and titanite U-Pb geochronology from the North Minwun Basin, Myanmar. *Geology*, **47**, 1–5, https://doi.org/10.1130/G46321.1/4679542/g46321.pdf.

Morley, C.K. & Racey, A. 2011. Tertiary Stratigraphy. *In*: Ridd, M. F., Barber, A. J. & Crow, M. J. (eds) *The Geology of Thailand*. London, The Geological Society, 223–271.

Morley, C.K. & Westaway, R. 2006. Subsidence in the super-deep Pattani and Malay basins of Southeast Asia: A coupled model incorporating lower-crustal flow in response to post-rift sediment loading. *Basin Research*, **18**, 51–84, https://doi.org/10.1111/j.1365-2117.2006.00285.x.

Morley, C.K., Sangkumarn, N., Hoon, T.B., Chonglakmani, C. & Lambiase, J. 2000. Structural evolution of the Li Basin, northern Thailand. *Journal of the Geological Society London*, **157**, 483–492.

Morley, C.K., Woganan, N., Sankumarn, N., Hoon, T.B., Alief, A. & Simmons, M. 2001. Late Oligocene–Recent stress evolution in rift basins of northern and central Thailand: implications for escape tectonics. *Tectonophysics*, **334**, 115–150, https://doi.org/10.1016/S0040-1951(00)00300-0.

Morley, C.K., Haranya, C., Phoosongsee, W., Pongwapee, S., Kornsawan, A. & Wonganan, N. 2004. Activation of rift oblique and rift parallel pre-existing fabrics during extension and their effect on deformation style: examples from the rifts of Thailand. *Journal of Structural Geology*, **26**, 1803–1829, https://doi.org/10.1016/j.jsg.2004.02.014.

Morley, C.K., Smith, M., Carter, A., Charusiri, P. & Chantraprasert, S. 2007. Evolution of deformation styles at a major restraining bend, constraints from cooling histories, Mae Ping fault zone, western Thailand. *Geological Society, London, Special Publications*, **290**, 325–349, https://doi.org/10.1144/SP290.12.

Morley, C.K., Charusiri, P. & Watkinson, I. 2011. Structural geology of Thailand during the Cenozoic. *In*: Ridd, M. F., Barber, A. J. & Crow, M. J. (eds) *The Geology of Thailand*. The Geological Society of London, 273–334.

Nachtergaele, S., Glorie, S., Charusiri, P., Kanjanapayont, P. & De Grave, J. 2017. Cenozoic exhumation of basement rocks in Thailand: constraints from apatite fission track and apatite (U-Th)/He thermochronology. *In*: *16th Gondwana International Conference*. Bangkok, Thailand.

Nachtergaele, S., De Pelsmaeker, E., et al. 2018. Meso-Cenozoic tectonic evolution of the Talas-Fergana region of the Kyrgyz Tien Shan revealed by low-temperature basement and detrital thermochronology. *Geoscience Frontiers*, **9**, 1495–1514, https://doi.org/10.1016/j.gsf.2017.11.007.

Nantasin, P., Hauzenberger, C., Liu, X., Krenn, K., Dong, Y., Thöni, M. & Wathanakul, P. 2012. Occurrence of the high grade Thabsila metamorphic complex within the low grade Three Pagodas shear zone, Kanchanaburi Province, western Thailand: Petrology and geochronology. *Journal of Asian Earth Sciences*, **60**, 68–87, https://doi.org/10.1016/j.jseaes.2012.07.025.

Ngah, K., Madon, M. & Tjia, H.D. 1996. Role of pre-Tertiary fractures in formation and development of the Malay and Penyu basins. *Geological Society, London, Special Publications*, **106**, 281–289, https://doi.org/10.1144/GSL.SP.1996.106.01.18.

Pal, T. 2011. Petrology and geochemistry of the Andaman ophiolite: melt – rock interaction in a suprasubduction-zone setting. *Journal of the Geological Society*, **168**, 1031–1045, https://doi.org/10.1144/0016-76492009-152.Petrology.

Palin, R.M., Searle, M.P., Morley, C.K., Charusiri, P., Horstwood, M.S.A. & Roberts, N.M.W. 2013. Timing of metamorphism of the Lansang gneiss and implications for left-lateral motion along the Mae Ping (Wang Chao) strike-slip fault, Thailand. *Journal of Asian Earth Sciences*, **76**, 120–136, https://doi.org/10.1016/j.jseaes.2013.01.021.

Pedersen, R.B., Searle, M.P., Carter, A. & Bandopadhyay, P.C. 2010. U–Pb zircon age of the Andaman ophiolite: implications for the beginning of subduction beneath the Andaman – Sumatra arc. *Journal of the Geological Society*, **167**, 1105–1112, https://doi.org/10.1144/0016-76492009-151.U.

Pubellier, M. & Morley, C.K. 2014. The basins of Sundaland (SE Asia): Evolution and boundary conditions. *Marine and Petroleum Geology*, **58**, 555–578, https://doi.org/10.1016/j.marpetgeo.2013.11.019.

Putthapiban, P. 1984. *Geochemistry, Geochronology and Tin Mineralization (Unpublished PhD Thesis)*. Chiang Mai University.

Qian, X., Feng, Q., Wang, Y., Zhao, T., Zi, J.W., Udchachon, M. & Wang, Y. 2017. Late Triassic post-collisional granites related to Paleotethyan evolution in SE Thailand: Geochronological and geochemical constraints. *Lithos*, **286–287**, 440–453, https://doi.org/10.1016/j.lithos.2017.06.026.

Racey, A. 2011. Petroleum Geology. *In*: Ridd, M. F., Barber, A. J. & Crow, M. J. (eds) *The Geology of Thailand*. The Geological Society of London, 351–392.

Racey, A., Duddy, I.R. & Love, M.A. 1997. Apatite fission track analysis of Mesozoic red beds from northeastern Thailand and western Laos. *In*: *The International Conference on Stratigraphy and Tectonic Evolution of Southeast Asia and the South Pacific Bangkok, Thailand, 19-24 August 1997*. 200–209.

Ridd, M.F. 2009. The Phuket Terrane: A Late Palaeozoic rift at the margin of Sibumasu. *Journal of Asian Earth Sciences*, **36**, 238–251, https://doi.org/10.1016/j.jseaes.2009.06.006.

Ridd, M.F. 2012. The role of strike-slip faults in the displacement of the Palaeotethys suture zone in Southeast Thailand. *Journal of Asian Earth Sciences*, **51**, 63–84, https://doi.org/10.1016/j.jseaes.2012.01.018.

Ridd, M.F. 2015. East flank of the Sibumasu block in NW Thailand and Myanmar and its possible northward continuation into Yunnan: A review and suggested tectono-stratigraphic interpretation. *Journal of Asian Earth Sciences*, **104**, 160–174, https://doi.org/10.1016/j.jseaes.2014.01.023.

Ridd, M.F. & Morley, C.K. 2011. The Khao Yai Fault on the southern margin of the Khorat Plateau, and the pattern of faulting in Southeast Thailand. *Proceedings of the Geologists' Association*, **122**, 143–156, https://doi.org/10.1016/j.pgeola.2010.08.008.

Sautter, B., Pubellier, M., Jousselin, P., Dattilo, P., Kerdraon, Y., Choong, C.M. & Menier, D. 2017. Late Paleogene rifting along the Malay Peninsula thickened crust. *Tectonophysics*, **710–711**, 205–224, https://doi.org/10.1016/j.tecto.2016.11.035.

Schmidt, W.J., Hoang, B.H., Handschy, J.W. & Hai, V.T. 2019. Tectonic evolution and regional setting of the Cuu Long Basin , Vietnam. *Tectonophysics*, **757**, 36–57, https://doi.org/10.1016/j.tecto.2019.03.001.

Searle, M.P. & Morley, C.K. 2011. Tectonic and thermal evolution of Thailand in the regional context of SE Asia. *In*: Ridd, M. F., Barber, A. J. & Crow, M. J. (eds) *The Geology of Thailand*. The Geological Society of London, 539–571.

Searle, M.P., Noble, S.R., Cottle, J.M., Waters, D.J., Mitchell, A.H.G., Hlaing, T. & Horstwood, M.S.A. 2007. Tectonic evolution of the Mogok metamorphic belt, Burma (Myanmar) constrained by U-Th-Pb dating of metamorphic and magmatic rocks. *Tectonics*, **26**, https://doi.org/10.1029/2006TC002083.

Searle, M.P., Whitehouse, M.J., et al. 2012. Tectonic evolution of the Sibumasu-Indochina terrane collision zone in Thailand and Malaysia: constraints from new U-Pb zircon chronology of SE Asian tin granitoids. *Journal of the Geological Society*, **169**, 489–500, https://doi.org/10.1144/0016-76492011-107.

Sibuet, J.C., Yeh, Y.C. & Lee, C.S. 2016. Geodynamics of the South China Sea. *Tectonophysics*, **692**, 98–119, https://doi.org/10.1016/j.tecto.2016.02.022.

Smith, M., Chantraprasert, S., Morley, C.K. & Cartwright, I. 2007. Structural geometry and timing of deformation in the Chainat duplex, Thailand. *Geological Society, London, Special Publications*, **290**, 305–323, https://doi.org/10.1144/SP290.11.

Sone, M. & Metcalfe, I. 2008. Parallel Tethyan sutures in mainland Southeast Asia: New insights for Palaeo-Tethys closure and implications for the Indosinian orogeny. *Comptes Rendus - Geoscience*, **340**, 166–179, https://doi.org/10.1016/j.crte.2007.09.008.

Sone, M., Metcalfe, I. & Chaodumrong, P. 2012. The Chanthaburi terrane of southeastern Thailand: Stratigraphic confirmation as a disrupted segment of the Sukhothai Arc. *Journal of Asian Earth Sciences*, **61**, 16–32, https://doi.org/10.1016/j.jseaes.2012.08.021.

Srisuriyon, K. & Morley, C.K. 2014. Pull-apart development at overlapping fault tips: Oblique rifting of a Cenozoic continental margin, northern Mergui Basin, Andaman Sea. *Geosphere*, **10**, 80–106, https://doi.org/10.1130/GES00926.1.

Stockli, D.F., Farley, K.A. & Dumitru, T.A. 2000. Calibration of the apatite (U-Th)/He thermochronometer on an exhumed fault block, White Mountains, California. *Geology*, **28**, 983–986.

Tingay, M., Morley, C., King, R., Hillis, R., Coblentz, D. & Hall, R. 2010. Present-day stress field of

Southeast Asia. *Tectonophysics*, **482**, 92–104, https://doi.org/10.1016/j.tecto.2009.06.019.

Tjia, H.D. 1994. Inversion tectonics in the Malay Basin: evidence and timing of events. *Geol. Soc. Malaysia, Bulletin 56*, 119–126.

Upton, D. 1999. *A Regional Fission Track Study in Thailand: Implications for Thermal History and Denudation (Unpublished PhD Thesis)*. Birkbeck and University College London.

Van Ranst, G., Pedrosa-Soares, A.C., Novo, T., Vermeesch, P. & De Grave, J. 2019. New insights from low-temperature thermochronology into the tectonic and geomorphologic evolution of the south-eastern Brazilian highlands and passive margin. *Geoscience Frontiers*, https://doi.org/https://doi.org/10.1016/j.gsf.2019.05.011.

Vermeesch, P. 2009. RadialPlotter: A Java application for fission track, luminescence and other radial plots. *Radiation Measurements*, **44**, 409–410, https://doi.org/10.1016/j.radmeas.2009.05.003.

Wagner, G.A. & Van den haute, P. 1992. *Fission-Track Dating*. Springer.

Watkinson, I., Elders, C. & Hall, R. 2008. The kinematic history of the Khlong Marui and Ranong Faults, southern Thailand. *Journal of Structural Geology*, **30**, 1554–1571, https://doi.org/10.1016/j.jsg.2008.09.001.

Watkinson, I., Elders, C., Batt, G., Jourdan, F., Hall, R. & McNaughton, N.J. 2011. The timing of strike-slip shear along the Ranong and Khlong Marui faults, Thailand. *Journal of Geophysical Research: Solid Earth*, **116**, 1–26, https://doi.org/10.1029/2011JB008379.

Wildman, M., Brown, R., et al. 2017. Contrasting Mesozoic evolution across the boundary between on and off craton regions of the South African plateau inferred from apatite fission track and (U-Th-Sm)/He thermochronology. *Journal of Geophysical Research: Solid Earth*, **122**, 1517–1547, https://doi.org/10.1002/2016JB013478.

Zeitler, P., Herczeg, A.L., Mcdougall, I. & Honda, M. 1987. U-Th-He dating of apatite: A potential thermochronometer. *Geochimica et Cosmochimica Acta*, **51**, 2865–2868.

Figure captions

Fig. 1. Overview of South East Asia in its plate-tectonic context. The major strike-slip faults, trenches and tectonic plates are indicated in black. The national borders of Thailand are indicated in white. The purple rectangle indicates the location of Fig. 3. Adapted from Simons et al. (2007) and Metcalfe (2013).

Fig. 2. (**a**) Tectonic subdivision and the distinct granite provinces in Thailand and surrounding countries. Major faults discussed in the text are indicated in red. The suture zones between different terranes are also shown. Adapted from Gardiner et al. (2016). (**b**) Structural map of Thailand with the indication of the complex fault network (black lines), basins (yellow), metamorphic core complexes (red) and Cenozoic folds in the Khorat Group. The study area, illustrated in Fig. 5, is visualized with a grey rectangle. Adapted from Morley (2015) and Morley et al. (2011).

Fig. 3. Topographic map of south-eastern Thailand with the analysed samples indicated by yellow dots. The few previously analysed samples of Upton (1999) (THI-numbers) close to the edge of the Khorat Plateau are also shown. Mapped Cenozoic strike-slip faults based on satellite images, outcrops and potential field data are illustrated with red lines.

Fig. 4. Examples of strike-slip fault zones from the study area in outcrop. (**a**) Google Earth image of NNW-SSE trending strike-slip fault in Palaeozoic sedimentary rocks south of Chantaburi, 12°31'47"N, 102°08'05"E. (**b**) Strike-slip fault in small quarry (see map A for location). (**c**) Google Earth image of aggregate quarry in metamorphic rocks SW of Khao Chao 13°13'56"N, 101°16'14"E. (**d**) View of quarry to SE showing the main lithologies cut by the brittle strike-slip fault, see map C for location. (**e**) Splays of the strike-slip fault in garnet biotite schist, juxtaposed with migmatites (see D for location). (**f**) Weathered part of strike-slip fault zone, showing internal folds and reverse faults (see D for location).

Fig. 5. Detailed geological map (based on Sone et al. (2012) and references therein) with sample locations and results of apatite fission track (AFT) and apatite (U-Th)/He (AHe) dating. The brown lines indicate fault splays of the Three Pagodas fault zone; the grey lines indicate fault splays from the Mae Ping Fault zone (based on Ridd and Morley, 2011). For location, see Fig. 2a and 2b.

Fig. 6. Confined fission track length histograms of the analysed samples (for locations, see Fig. 3). The number of measured confined tracks and the length (in µm) is indicated on the vertical and horizontal axis, respectively. Mean track lengths (l_m), standard deviation (σ) and number of tracks (n) are displayed. Most confined track length data consists of less than 40 confined track length measurements, due to a low density of spontaneous tracks in the etched apatite grains. Hence, Cf-irradiation were performed on separate mounts for samples KM-04, KM-07, KM-09, KM-14A, KM-14B and KM-15 and subsequent measurement results were added. Some samples with sufficient length measurements (>100) will be used for thermal history modelling in Figure 7, following the recommendations of Barbarand *et al.* (2003). Samples with more than 40 length measurements were modelled and can be found in Appendix 5.

Fig. 7. Time-temperature reconstructions or thermal history models (left) for NT-02 (upper) and KM-14B (lower), reconstructed with the QTQt modelling software (Gallagher 2012). The colour-scale

indicates relative probability for residence at that particular time-temperature point in geological time. The input parameters from the confined track length measurements and fit of the most likelihood model are given in the middle panel. The predicted and observed values for the kinetic parameter, apatite fission track age and mean track length are shown in the right panel.

Fig. 8. Evolution of the intracratonic basins and major fault zones of southern Thailand, adapted from (Morley 2015). The blue arrows indicate the sense of strike-slip movement of the major strike-slip faults. All information below the figures are extracted from the literature. Sources were cited in geological setting of this paper.

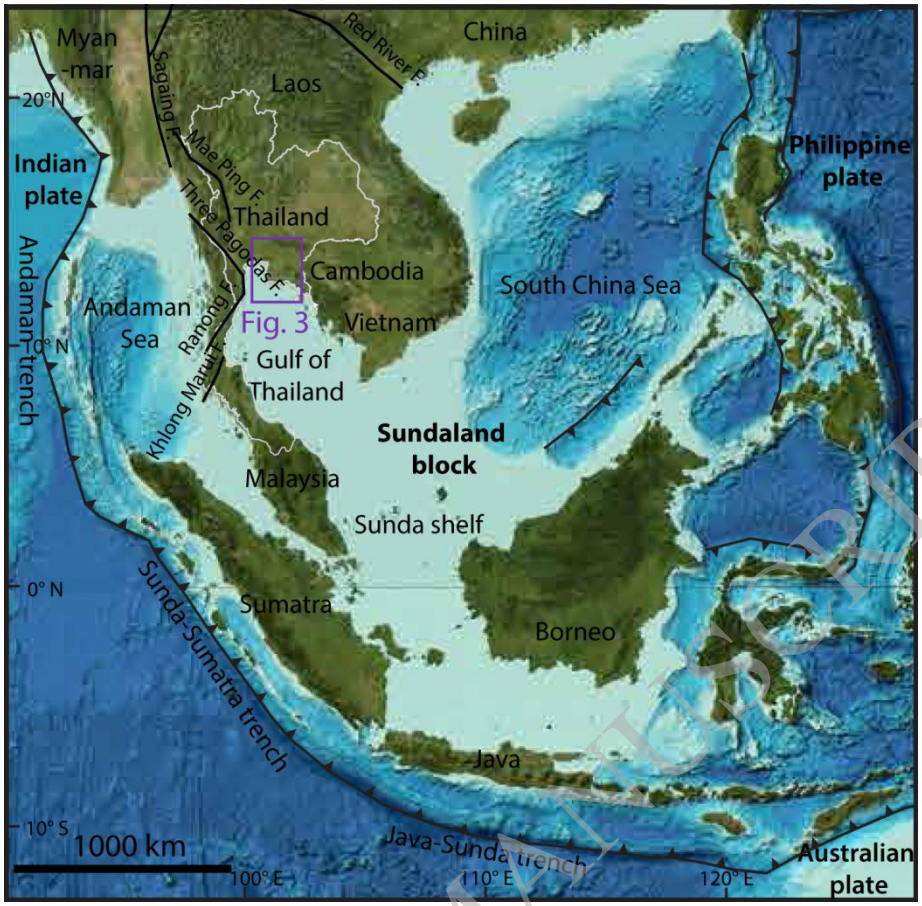

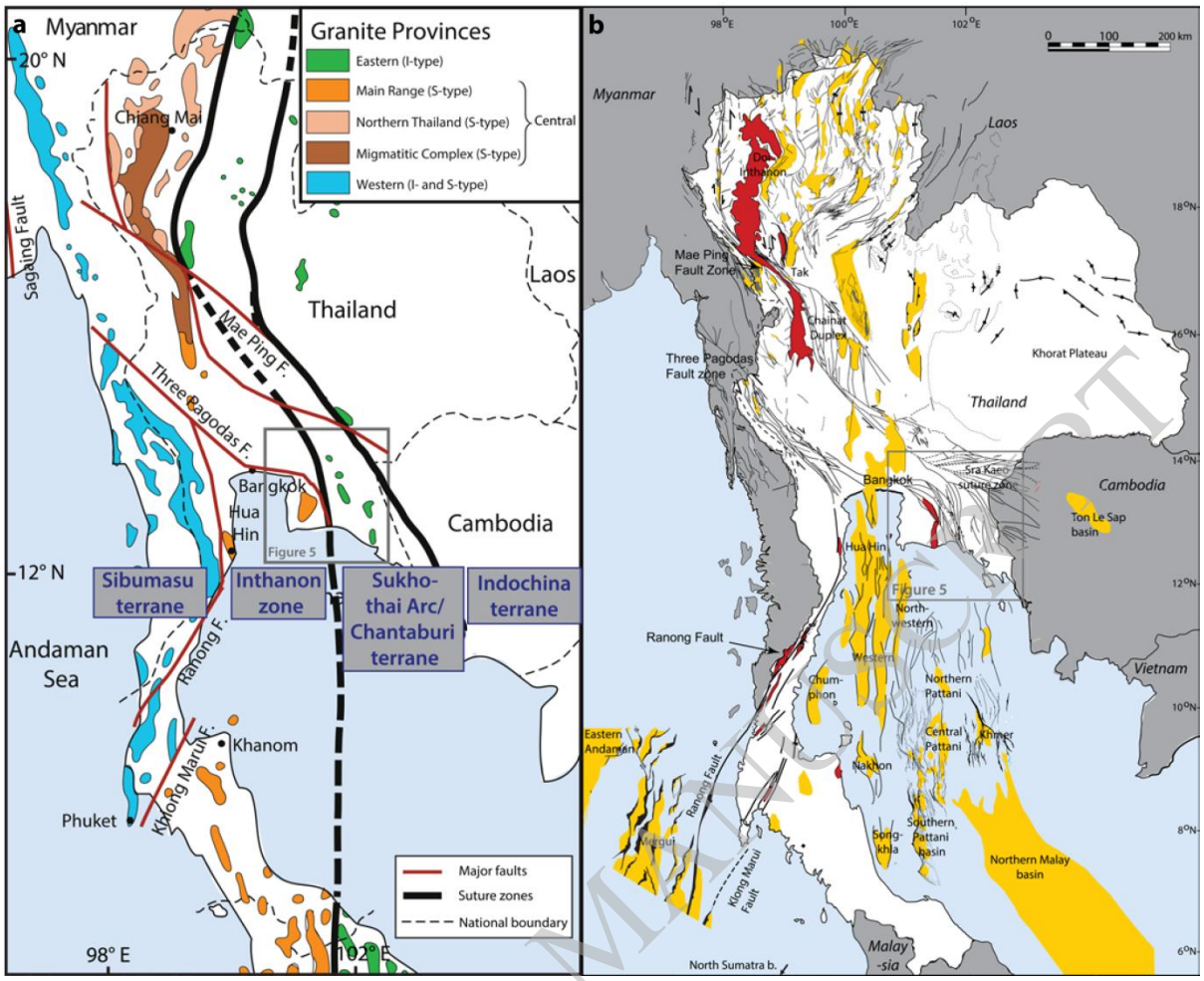

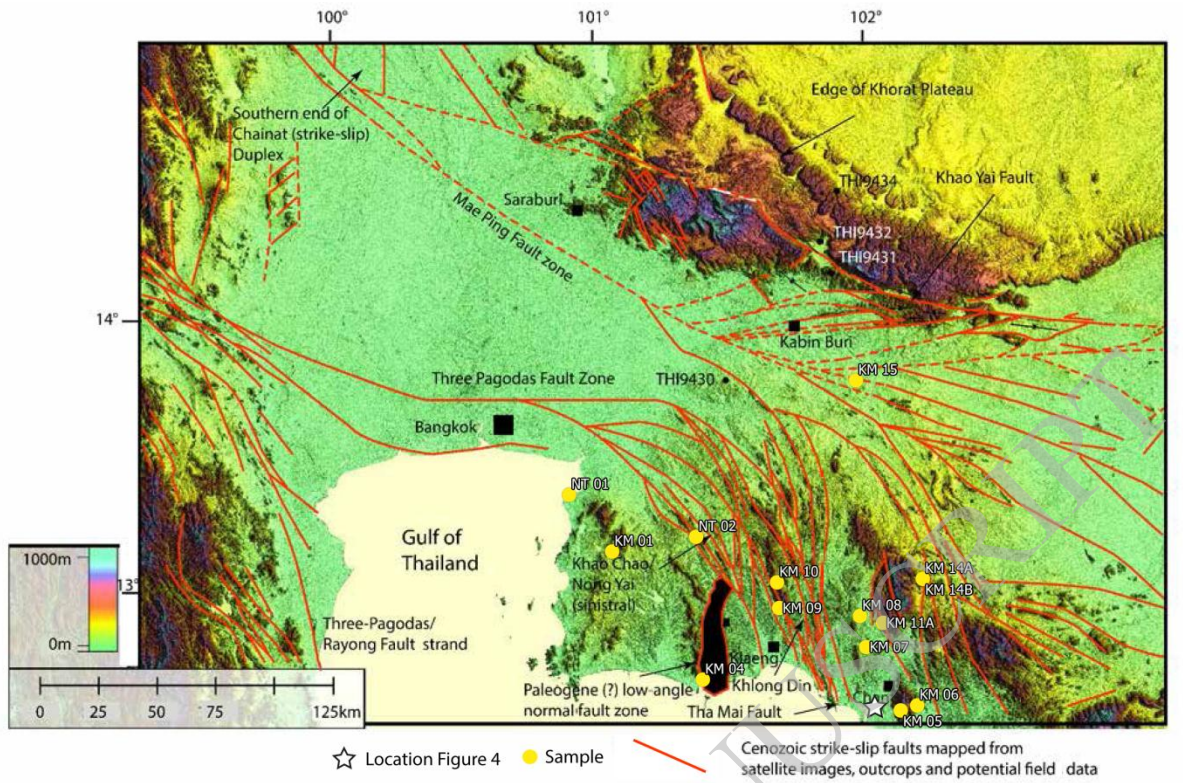

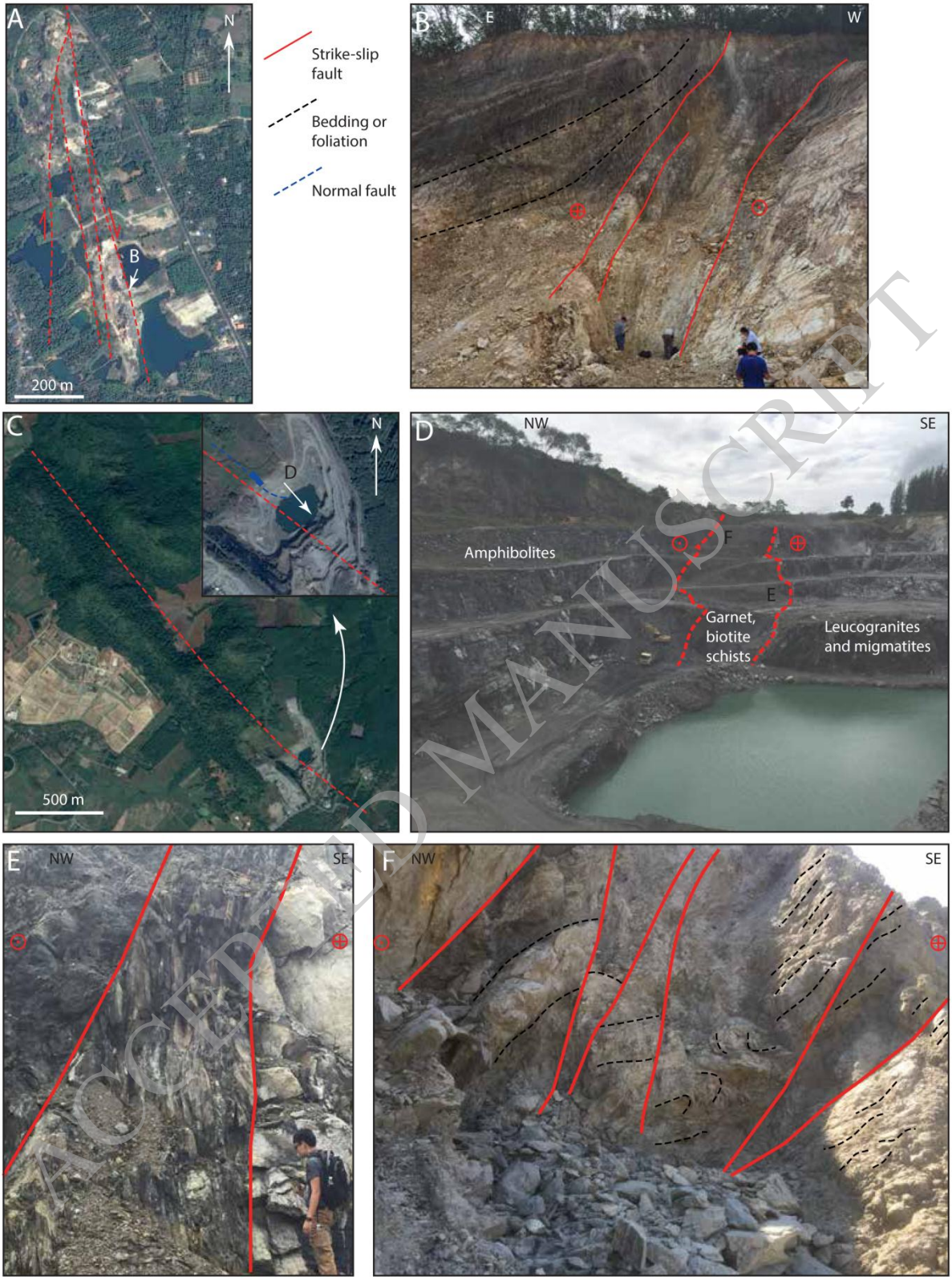

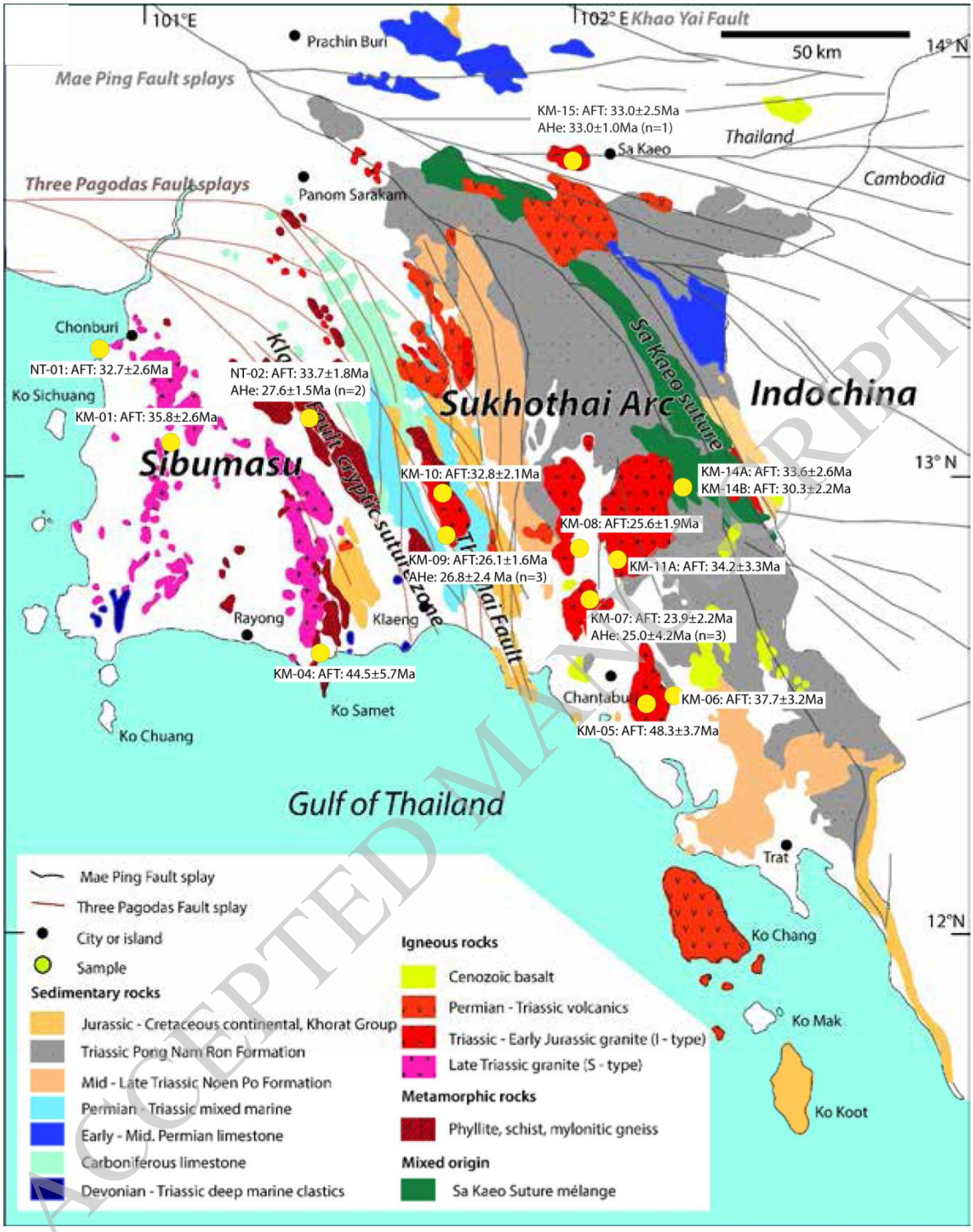

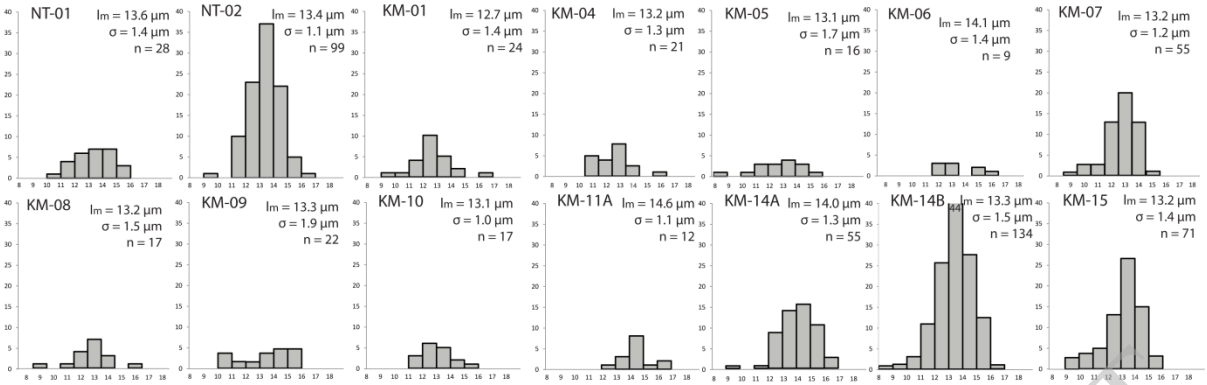

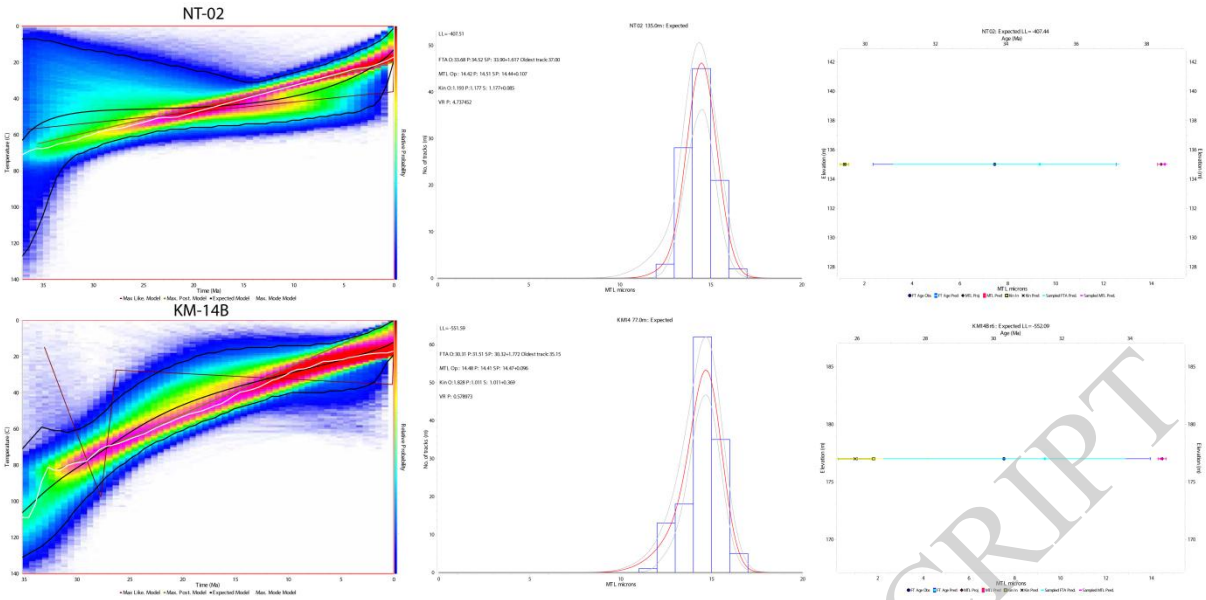

Late Eocene - earliest Oligocene (40-30 Ma)

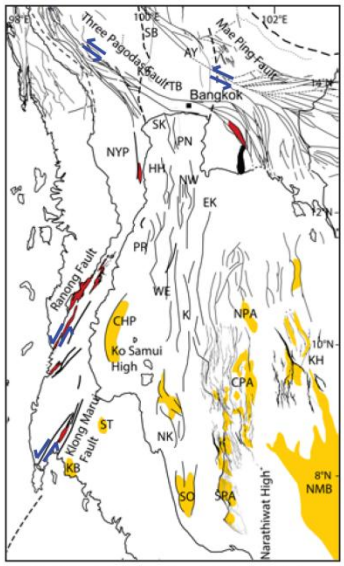

- sinistral strike slip brittle faulting of the Mae Ping fault, Three Pagodas fault, Ranong fault and Khlong Marui fault
- rift phase of southern and eastern basins of the Gulf of Thailand
- main cooling phase of basement rocks in Southeastern Thailand

latest Early Oligocene - Late Oligocene (30-24 Ma)

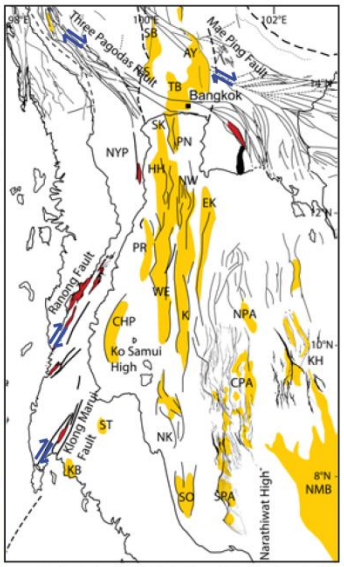

- dextral strike-slip brittle faulting of the Mae Ping fault and Three Pagodas fault
- basins in northwestern Gulf of Thailand start rifting
- basins in southern Gulf of Thailand continue rifting
- some basement rock cooling is observed in southeastern Thailand

Oligocene - Miocene transition (23 Ma)

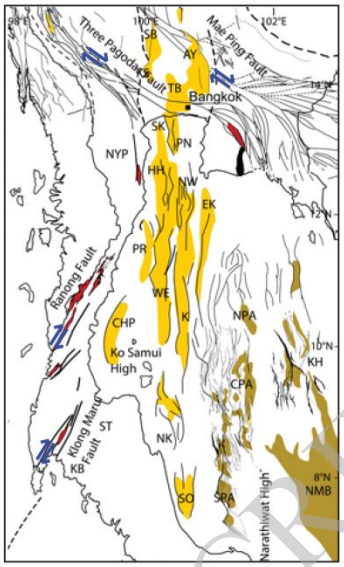

- dextral strike-slip brittle faulting of all main faults resulting in final exhumation in Peninsular Thailand but had only minor influence on Southeastern Thailand
- all basins in Gulf of Thailand experience a phase of uplift around 23 Ma
- rifting generally only continues in basins of central and northern Thailand
- post-rift phase initiates in southeastern Gulf of Thailand

Figure explanation

NS	Nakhon Sawan
SB	Suphan Buri
AY	Ayutthaya
KS	Kamphaeng Saen
TB	Thon Buri
SK	Sakhon
PN	Paknam
HH	Hua Hin
NW	Northwestern
WE	Western
K	Kra
EK	East Kra
NP A	North Pattani
CP A	Central Pattani
SP A	South Pattani
KH	Khmer
PR	Prachuap
CHP	Chumphon
NK	Nakhon
MER	Mergui
SO	Songkhla
MA	Mergui
KB	Krabi
NMB	North Malay Basin
ST	Surat Thani
NYP	Nong y Plong
EA	East Andaman

Cenozoic strike-slip or normal fault

Basin in syn-rift phase

Basin in post-rift phase

Deformed granite-gneiss that may display Cenozoic metamorphism and migmatites

Cenozoic folds in Khorat Group

Table 1. Sample localities

Sample	Latitude	Longitude	Altitude	Lithology	Pluton	Analyses
NT 01	N 13°20'22.5"	E 100°55'28.8"	1 m	biotite granite	Chonburi	AFT
NT 02	N 13°10'50.7"	E 101°24'17.0"	135 m	gneiss	Ban Na Cham	AFT, AHe
KM 01	N 13° 07.510'	E 101° 05.238'	140 m	biotite granite	Rayong	AFT
KM 04	N 12° 38.485'	E 101° 25.789'	28 m	metagranite (foliated)	Ban Na Cham	AFT
KM 05	N 12° 31.492'	E 102° 10.652'	46 m	granodiorite	Chantaburi	AFT
KM 06	N 12° 32.635'	E 102° 14.401'	51 m	granite	Chantaburi	AFT
KM 07	N 12° 45.868'	E 102° 02.834'	40 m	granodiorite	Khao Cha Mao	AFT, AHe
KM 08	N 12° 52.919'	E 102° 01.414'	57 m	granite	Khao Cha Mao	AFT
KM 09	N 12° 54.707'	E 101° 43.120'	100 m	granite (sheared)	Nong Yai	AFT, AHe
KM 10	N 13° 00.515'	E 101° 42.617'	87 m	granite	Nong Yai	AFT
KM 11A	N 12° 51.358'	E 102° 06.658'	70 m	granite	Klathing	AFT
KM 14A	N 13° 01.321'	E 102° 15.648'	177 m	granite	Klathing	AFT
KM 14B	N 13° 01.321'	E 102° 15.648'	177 m	granite	Klathing	AFT
KM 15	N 13° 46.300'	E 102° 00.518'	56 m	migmatized granite	Sa Kaeo	AFT, AHe

Sample localities and lithology with indication of techniques used: apatite fission track (AFT) and/or apatite (U-Th)/He (AHe)

Table 2. Apatite Fission Track (AFT) data

Sample	n	ρ_s (± 1σ)	N_s	ρ_i (± 1σ)	N_i	[U]	ρ_d (± 1σ)	N_d	ρ_s/ρ_i (± 1σ)	P(χ^2)	Disp.	t_ζ	t_c	l_m	n_l	σ	D_{par}
NT 01	25	4.772 (0.226)	262	9.594 (0.409)	551	25.2	4.822 (0.098)	2411	0.508 (0.038)	0.96	0.0036	35.0 ± 2.8	32.7 ± 2.6	13.6	28	1.4	1.37
NT 02	20	8.302 (0.320)	672	16.836 (0.320)	1373	44.2	4.822 (0.098)	2411	0.520 (0.024)	0.40	0.52	35.8 ± 1.9	33.7 ± 1.8	13.4	99	1.1	1.23
KM 01	23	9.538 (0.399)	571	18.548 (0.550)	1138	46.9	5.017 (0.100)	2508	0.533 (0.027)	0.03	19.6	38.2 ± 2.2	35.8 ± 2.6	12.7	24	1.4	1.20
KM 04*	23	2.641 (0.150)	271	4.901 (0.213)	532	12.0	5.169 (0.102)	2581	0.749 (0.056)	0.00	45.4	*55.1 ± 4.2*	*44.5 ± 5.7*	13.2	21	1.3	1.12
KM 05	20	4.570 (0.254)	325	6.718 (0.301)	496	17.5	5.026 (0.100)	2513	0.643 (0.046)	0.65	2.43	46.1 ± 3.5	48.3 ± 3.7	13.1	16	1.7	1.17
KM 06	19	2.361 (0.154)	234	2.361 (0.154)	458	11.2	5.168 (0.102)	2584	0.541 (0.043)	0.40	1.35	39.9 ± 3.3	37.7 ± 3.2	14.1	9	1.4	1.24
KM 07*	20	2.754 (0.169)	265	8.667 (0.302)	822	21.2	5.174 (0.102)	2587	0.336 (0.024)	0.24	19.6	24.8 ± 1.8	23.9 ± 2.2	13.2	55	128	1.28
KM 08	25	3.040 (0.177)	296	8.655 (0.296)	853	21.2	5.180 (0.102)	2590	0.363 (0.024)	0.89	3.6	26.8 ± 1.9	25.6 ± 1.9	13.2	17	1.5	1.23
KM 09*	25	1.196 (0.097)	150	3.302 (0.160)	425	8.1	5.188 (0.102)	2594	0.401 (0.038)	0.79	0.097	29.7 ± 2.9	26.1 ± 2.6	13.3	22	1.9	1.33
KM 10	29	3.368 (0.165)	415	7.507 (0.246)	934	18.9	5.030 (0.100)	2515	0.464 (0.027)	0.85	5.40	33.3 ± 2.1	31.9 ± 2.1	13.1	17	1.0	1.13
KM 11A	10	11.484 (0.578)	395	24.249 (0.834)	846	59.2	5.194 (0.102)	2597	0.490 (0.030)	0.03	18.5	36.3 ± 2.3	34.2 ± 3.3	14.6	12	1.1	1.55
KM 14A*	20	2.999 (0.182)	271	6.569 (0.269)	297	16.0	5.206 (0.102)	2603	0.481 (0.035)	0.35	3.76	35.8 ± 2.7	33.6 ± 2.6	14.0	55	1.3	1.81
KM 14B*	20	3.630 (0.177)	422	8.767 (0.271)	1044	21.3	5.212 (0.102)	2606	0.433 (0.025)	0.08	15.8	32.2 ±1.9	30.3 ± 2.2	13.3	134	1.5	1.83
KM 15*	25	3.111 (0.187)	278	6.283 (0.251)	627	15.3	5.218 (0.102)	2609	0.511 (0.037)	0.73	0.92	38.0 ± 2.8	33.0 ± 2.5	13.2	71	1.4	1.38

Apatite fission track data of basement apatites from south-eastern Thailand: *n* grains were analysed for each sample. ρ_s and ρ_i represent the areal density of the etched spontaneous and induced fission tracks (measured in the external detector) respectively. N_s and N_i correspond to the number of counted spontaneous and induced fission tracks. [U] indicates the mean Uranium concentration of the analysed grains using the appropriate formula (Enkelmann *et al.* 2005). ρ_d values are linearly interpolated values of the track density in the external detector attached to the Uranium-doped glass dosimeters (IRMM-540, De Corte et al., 1998). ρ_s, ρ_i and ρ_d values are expressed as 10^5 tracks/cm². P(χ^2) represents the chi-squared probability that the ρ_s/ρ_i ratio is constant. The degree of dispersion is also shown. Zeta t_ζ and central ages t_c are given for each sample (in Ma). The mean track lengths (l_m) are based on limited numbers (n_l) of confined track length measurements. Samples indicated with * benefited from ^{252}Cf irradiation in order to increase the number of confined track length measurements. The standard deviation on the confined track length distribution (σ) and the etch pit diameter (D_{par}) is also reported. All samples were analysed by S. Nachtergaele who has a personal zeta-factor of 286.2 ± 4.7 a*cm² calibrated on multiple Durango and Fish Canyon Tuff age standards and the IRMM-540 glass -(De Corte *et al.* 1998).

Table 3. Apatite (U-Th)/He data

Sample	Geometry	U (ppm)	σ	Th (ppm)	σ	He (pmol)	He err (%)	eU	σ	$F_T(^{238}U)$	$F_T(^{235}U)$	$F_T(^{232}Th)$	Unc. age (Ma)	σ	Cor. Age (Ma)	σ	Weighte
NT 02 (3)	cylindrical	40.205	0.432	9.23	0.1	0.01301	0.00023	42.37	0.433	0.757	0.721	0.715	19.144	0.398	**25.4**	0.527	**27.6 Ma (1.5 Ma; 2)**
NT 02 (4)	hexagon 1T	21.04	0.224	2.655	0.027	0.058	0.00015	21.66	0.224	0.863	0.842	0.839	25.614	0.272	**29.7**	0.316	
KM 07 (1)	hexagon 2T	69.396	0.625	137.5318	0.9788	0.0123	0.00022	101.7	0.666	0.731	0.69	0.684	10.889	0.212	**15.2**	0.297	
KM 07 (2)	hexagon 0T	22.925	0.328	72.441	0.778	0.01215	0.00023	39.94	0.376	0.698	0.654	0.648	22.01	0.467	**32.6**	0.693	
KM 07 (3)	hexagon 2T	37.596	0.382	87.546	0.667	0.01689	0.00024	58.17	0.413	0.751	0.713	0.708	20.248	0.32	**27.6**	0.436	**25.02 Ma (4.19 Ma;3)**
KM 07 (4)	hexagon 1T	19.46	0.428	75.268	0.839	0.00543	0.00022	37.14	0.471	0.656	0.607	0.599	24.44	1.03	**38.9**	1.64	
KM 09 (1)	hexagon 2T	1.15	0.3	26.925	0.294	*0.00086*	*0.00021*	7.48	0.3	0.64	0.588	0.58	25.61	6.31	**43**	11	
KM 09 (2)	hexagon 1T	1.82	0.13	13.22	0.117	0.00133	0.00021	4.92	0.13	0.718	0.676	0.67	18.88	3.09	**27.5**	4.5	
KM 09 (3)	hexagon 0T	1.66	0.12	18.817	0.182	0.00104	0.00021	6.09	0.13	0.689	0.644	0.637	14.86	3.1	**22.8**	4.76	**26.8 Ma (2.4 Ma; 3)**
KM 09 (4)	cylindrical	4.38	0.2	17.658	0.18	0.00176	0.00021	8.53	0.2	0.705	0.661	0.655	19.63	2.44	**28.9**	3.6	
KM 15 (1)	hexagon 2T	33.461	0.343	142.007	1.118	*0.1905*	*0.0014*	66.83	0.347	0.757	0.721	0.715	132.543	1.271	**179.6**	1.723	**Single grain age: 33.0 ± 1.0 Ma**
KM 15 (2)	hexagon 2T	25.372	0.391	83.933	0.711	0.00713	0.00022	45.09	0.324	0.672	0.624	0.617	21.398	0.695	**33.1**	1.07	
KM 15 (3)	hexagon 2T	16.602	0.407	27.806	0.3	*0.00196*	*0.00026*	23.13	0.304	0.639	0.586	0.578	16.52	2.24	**26.6**	3.61	
KM 15 (4)	hexagon 0T	74.18	4.96	373	19	*0.01185*	*0.00023*	161.8	6.797	0.744	0.707	0.701	3.53	0.16	**4.9**	0.23	

The concentrations and analytical uncertainty of the U, Th and He measurements are displayed for each aliquot. Uncorrected ages are subsequently corrected for He ejection based on the geometry and specific dimensions of the analyzed apatite crystal. Mean ages are calculated with IsoplotR (Vermeesch 2018). Incomplete degassed grains (e.g. KM 09 (1) and KM 15 (3)) and grains with anomalous ages (KM 15 (1), KM 15 (4)) were not used in this calculation.

Table 4. Apatite (U-Th)/He crystal dimensions and alpha-ejection corrected ages

Sample	Geometry	Height (µm)	Width (µm)	Thickness (µm)	Corrected age (Ma)	σ (Ma)	Corrected age (Ma)	σ (Ma)	δ (%)
					Appropriate geometry		*Hexagonal infinite slab*		
NT02 (3)	cylindrical	163.2	86.9	83.4	25.4	0.53	27.2	0.57	7.1%
NT02 (4)	hexagon 1T	252.0	227.0	186.1	29.7	0.32	29.6	0.32	0.4%
KM 07 (1)	hexagon 2T	142.1	114.9	96.6	15.2	0.30	14.9	0.29	2.4%
KM 07 (2)	hexagon 0T	196.3	76.15	74.4	32.6	0.69	33.2	0.71	2.0%
KM 07 (3)	hexagon 2T	158.6	116.9	107.9	27.5	0.44	27.1	0.43	1.6%
KM 07 (4)	hexagon 1T	109.4	76.2	71.7	38.9	1.64	39.7	1.67	2.0%
KM 09 (1)	hexagon 2T	108.4	80.0	68.6	43.0	11.0	43.0	11.0	0.0%
KM 09 (2)	hexagon 1T	193.0	88.4	72.9	27.5	4.50	27.9	4.57	1.5%
KM 09 (3)	hexagon 0T	166.0	76.0	72.0	22.8	4.76	23.5	4.89	2.7%
KM 09 (4)	cylindrical	182.9	66.8	63.1	28.9	3.60	31.9	3.98	10.6%
KM 15 (1)	hexagon 2T	244.2	100.3	89.0	179.6	1.72	181.0	1.74	0.8%
KM 15 (2)	hexagon 2T	157.7	75.4	66.9	33.1	1.07	33.5	1.09	1.3%
KM 15 (3)	hexagon 2T	132.7	67.3	68.2	26.6	3.61	26.9	3.65	1.1%
KM 15 (4)	hexagon 0T	193.2	99.0	82.3	4.9	0.23	5.0	0.23	1.4%

This geometry and exact dimensions are shown here for all analysed apatite crystals during apatite (U-TH)/He analysis. F_T-corrected ages are displayed for all the same hexagonal infinite slab geometry and for the appropriate geometry (displayed in the second column) using HelioCalc software (P. Vermeesch).